WIND MODELS FOR FLIGHT SIMULATOR CERTIFICATION OF LANDING AND APPROACH GUIDANCE AND CONTROL SYSTEMS

Dwight R. Schaeffer

FOREWORD

This paper is taken from Department of Transportation Report No. *FAA-RD-74-206,* December *1974,* having the same title, authored by Neal M. Barr, Dagfinn Gangsaas, and Dwight R. Schaeffer. Substantiation of information presented is provided in this report.

INTRODUCTION

This paper reports an investigation performed to provide the information for improved accuracy of low-altitude wind and turbulence models to be used for the certification by flight simulation of approach and landing guidance and control systems.

Historically, the structural designers were first to recognize the requirement for a mathematical model and initially used only the discrete 1-cosine gust for the design limit case. As airplanes became lighter and more flexible, fatigue life became more critical and the need for a more accurate description became greater. This led to the application of the statistical power spectra. Attempts to fit a mathematical model to measured data began seriously in the late 1950s and has progressed to the point of "which model do I use?"

Automatic controls were used initially to provide modest improvements of airplane stability and to provide guidance during noncritical flight phases (altitude, attitude, and heading hold). Automatic control authority tended to be low. Hence, the interaction of the control system with wind and turbulence was unimportant; it was not a concern for flight safety,

For typical flight controls analysis, such as handling qualities, ride qualities, and controllability, concern was for a qualitative, rather than quantitative, answer; that is, does a parameter variation (in the aircraft or control system) improve or degrade the particular output? A forced change in this philosophy occurred when the autoland systems began to appear in the early 1960s. The dependence upon an automatic landing system rather than the highly adaptive pilot required analytic proof that the landing would be

performed with adequate safety. The problem is now quantitative rather than qualitative and a gross error in the approach wind model could be very serious; parameters of the wind model have effects comparable to parameters of the aircraft and guidance system. Certification of autoland systems is dependent upon demonstration of very low orders or risk of fatal accidents. Obtaining adequate statistical data to validate remote probabilities of fatal accidents is impractical without heavy reliance upon simulation.

The search for a low-altitude wind model, providing a better representation of low-altitude wind phenomena than provided by existing certification wind models, was principally concerned with the region from the surface to about 1000 feet. The model for this altitude region tends to be the most general and complex due to the strong dependence of wind characteristics upon altitude and surface terrain and the orientation dependence of turbulence characteristics. Additionally, the landing approach task is the most difficult and critical task for which relatively small changes of wind characteristics may result in large changes in maneuver performance. The low airspeed during approach tends to couple vertical motion with longitudinal wind components and longitudinal motion with vertical wind components, increases the nonlinearity of aircraft responses to winds, and increases the significance of the distribution of winds over the aircraft. Hence, the aerodynamic model incorporating the effects of winds tends also to be most general and complex.

The main objective of the investigation was to define a model suitable for certification. A model for design must be simplified to reduce the wind model parameters to enable evaluation of a large number of aircraft and control system design parameters.

The studies were concerned with the "average" airport, although it is recognized that the "average" airport may not exist. It is both impractical and undesirable to represent unique characteristics of any particular airport for the certification of an aircraft that will land at many different airports. "Average" airport is used in regard to possible unique operating procedures and terrain features and does not imply "average" winds at the "average" airport.

Consideration is not for the wind alone, but for aircraft responses in wind environments, *so* the investigation included the representation of aerodynamic forces due to winds and a brief analysis of the effects of winds on aircraft motion.

No original work on the description of low-altitude winds is intended. The wind model is a combination of the work of others. The structure of the model has been parameterized to enable incorporation of new material and updating of parts without discarding the entire model.

For virtually every aspect of low-altitude winds there are conflicting descriptions. Some descriptions are based on undocumented data collection, analysis techniques, and test conditions. Some general considerations used for selecting one among competition descriptions are:

- Weight of evidence
- Physical and intuitive reasonableness
- Substantiation
- Existing specifications, when the choice appears arbitrary
- Compatibility with the description of other parameters
- Validity of the assumptions
- Avoidance of descriptions providing unreasonable discontinuities

Analytic descriptions of wind phenomena are presented. Where possible, a deterministic description is preferred in the presumption that all physical processes have cause-and-effect relationships. When relationships are too complex to permit quantitative understanding or when deterministic descriptions are impractical, probabilistic descriptions are used, with the statistical parameters defined deterministically as much as possible.

For those parameters defying analytic description, probabilistic descriptions have been sought. Probabilistic descriptions were first sought from the literature. For those aspects not well defined by the literature, descriptions have been sought by reducing and evaluating tower data.

A brief analysis of the effects of winds on aircraft motion has been conducted to gain an appreciation of what needs to be modeled. The axes transformations required between wind and turbulence components in their inherent axis system and in the airplane's axis system are shown. Techniques of providing a random process on computers for the representation of turbulence are presented. A simulation model is presented that combines all the foregoing components.

NOMENCLATURE

b	Wing span
C_p	Specific heat at 'constant pressure
$\bar{c}$	Mean chord
d	Atmospheric boundary layer thickness
e	Exponential function
f	Coriolis parameter, $f = 2\omega_E \sin \lambda$
$f(h/\ell')$	Contribution of nonneutral atmospheric stability to the mean wind
$f(\xi), g(\xi)$	Fundamental longitudinal and transverse correlation functions for isotropic turbulence, respectively
G_u, G_v, G_w	Filters for producing u, v, and w components of turbulence
g	Acceleration due to gravity
$g(h/\ell')$	Contribution of atmospheric stability to mean wind caused by variation of shear stress
H	Heat flux, positive upward
h	Altitude
h_{REF}	Reference altitude
h_I	Altitude above which turbulence is isotropic
k	von Karman constant, $k = 0.4$
L	Longitudinal isotropic turbulence integral scale

L_H, L_V	Integral scales for horizontal and vertical turbulence components
L_P, L_N	Longitudinal and transverse integral scales for turbulence components parallel and normal to the displacement vector, respectively
L_u, L_v, L_w	Integral scales corresponding to the longitudinal, transverse, and vertical turbulence components, respectively
ℓ, ℓ'	Monin-Obukov scaling length and Monin-Obukov scaling length modified by ratio of eddy conductivity to eddy viscosity
ℓ_T	Distance from the wing-body aerodynamic center to the tail aerodynamic center along the x body axis, positive aft
$M(\omega)$	Frequency response amplitude
p	Inertial body axis roll rate
p_T	Effective roll rate of the air mass due to turbulence relative to the earth
q	Inertial body axis pitch rate
$\bar{q}$	Dynamic pressure
q_T	Effective body axis pitch rate due to turbulence with respect to the earth
R_i, $R_{i_{20}}$	Richardson's number and that at 20-foot altitude
R_{ij}	Correlation for the i and j turbulence components
r	Inertial body axis yaw rate

$\vec{r}$	Displacement vector
r_A	Yaw rate relative to the air mass
r_T	Effective body axis yaw rate due to turbulence relative to the earth
$r_W, \bar{r}_W$	Effective yaw rate due to the wind and mean wind relative to the earth
s	Laplace transform variable
T	Absolute temperature
t	Time
u	Inertial linear velocity along the x body axis
u_*, u_{*_0}	Friction velocity (shear stress/density density)$^{1/2}$ and that at the surface
u_A	Linear velocity with respect to the air mass along the x body axis
$u_{A_{TG}}$	Component of airspeed along the x turbulence generation axis
u_P, u_N	Turbulence velocity parallel and normal to the displacement vector
$u_T, u_{T_{TG}}$	Linear turbulence velocity along the x body axis and the x turbulence generation axis relative to the earth
$u_{T_{TAIL}}$	u_T at the tail
$u_W, \bar{u}_W$	Linear velocity of the wind and mean wind with respect to the earth along the x body axis

$\bar{V}_W, \bar{V}_{20}$	Mean wind speed and that at 20-foot altitude
V_A	Total air speed
v	Inertial linear velocity along the y body axis relative to the earth
v_A	Linear velocity with respect to the air mass along the y body axis
$v_T, v_{T_{TG}}$	Linear turbulence velocity along the y body axis and the y turbulence generation axis relative to the earth at the center of gravity
$v_W, \bar{v}_W$	Linear velocity of the wind and mean wind along the y body axis relative to the earth
w	Inertial linear velocity along the *z* body axis
w_A	Linear velocity along the z body axis relative to the air mass
w_T	Linear turbulence velocity along the *z* body axis relative to the earth
w_W, w_W	Linear velocity of the wind and the mean wind along the z body axis relative to the earth
z_0	Surface roughness length
α	Angle of attack
β	Sideslip angle
γ	Glide slope
θ	Euler pitch angle

$\theta_{ij}(\vec{\Omega})$	Three-dimensional spectrum function for the i and j turbulence components
X	Latitude
λ_1, λ_2	Turbulence wavelength along the x and y axis
$\vec{\xi}, \xi$	Position displacement vector and magnitude
σ_i	Standard deviation for parameter i
σ_H, σ_V	Standard deviation of horizontal and vertical turbulence
$\sigma_u, \sigma_v, \sigma_w$	Standard deviations of the u, v, and w components of turbulence
σ_{ij}^2	Covariance between the i and j turbulence components
τ	Time displacement
τ, τ_0	Shear stress and that measured at the surface
Φ_I, Φ_O	Input and output power spectra
$\Phi_i(\Omega_1)$	One-dimensional power spectrum for parameter i
$\Phi_{ij}(\Omega_1)$	One-dimensional spectrum function for the i and j turbulence components
Φ_N	Random noise power spectrum
$\Phi_{NN}(\Omega_1), \Phi_{PP}(\Omega_1)$	Isotropic one-dimensional spectrum functions for u_N and u_P
$\Phi_u(\Omega_1), \Phi_v(\Omega_1), \Phi_w(\Omega_1)$	One-dimensional power spectra for components of turbulence along the x, y, and *z* axis

$\Phi_{uw}(\Omega_1)$	One-dimensional cospectrum for components of turbulence along the x and z axis
$\phi(h/\ell')$	Universal function of h/ℓ' defining nondimensional wind shear: $\frac{kh}{u_{*_0}} \frac{\partial \overline{V}_W}{\partial h} = \phi(h/\ell')$
ϕ	Euler bank angle
$\psi_{ij}(\Omega_1, \Omega_2)$	Two-dimensional spectrum function for the i and j turbulence components
ψ	Euler heading angle
$\overline{\psi}_W$	Heading to which the mean wind is blowing
$\vec{\Omega}, \Omega$	Spacial frequency vector and spacial frequency magnitude
Ω_1	Component of spacial frequency along the x axis
ω	Temporal frequency, rad/sec
	Angular velocity of the earth

Note: Dotted terms refer to derivatives with respect to time. Overbar indicates an average. Other terms defined where used.

WIND MODELS FOR FLIGHT SIMULATOR CERTIFICATION OF LANDING AND APPROACH GUIDANCE AND CONTROL SYSTEMS

Wind phenomena are classed as being mean wind, turbulence, and discrete gusts. Mean wind and turbulence are statistical parameters that appear together with turbulence being a random deviation of wind velocity about the mean. Distinction between the mean wind, which eventually is variable given enough time or space, is made on a frequency basis using the Van der Hoven bimodal wind speed spectrum (Fig. 1).

Discrete gusts are deterministic phenomena caused by localized terrain or atmospheric inhomogeneities of which there are an infinite number of possibilities. So long as conditions of reasonably homogeneous terrain and atmospheric features or restrictions on the proximity to inhomogeneities are justified, consideration of discrete gusts is unnecessary.

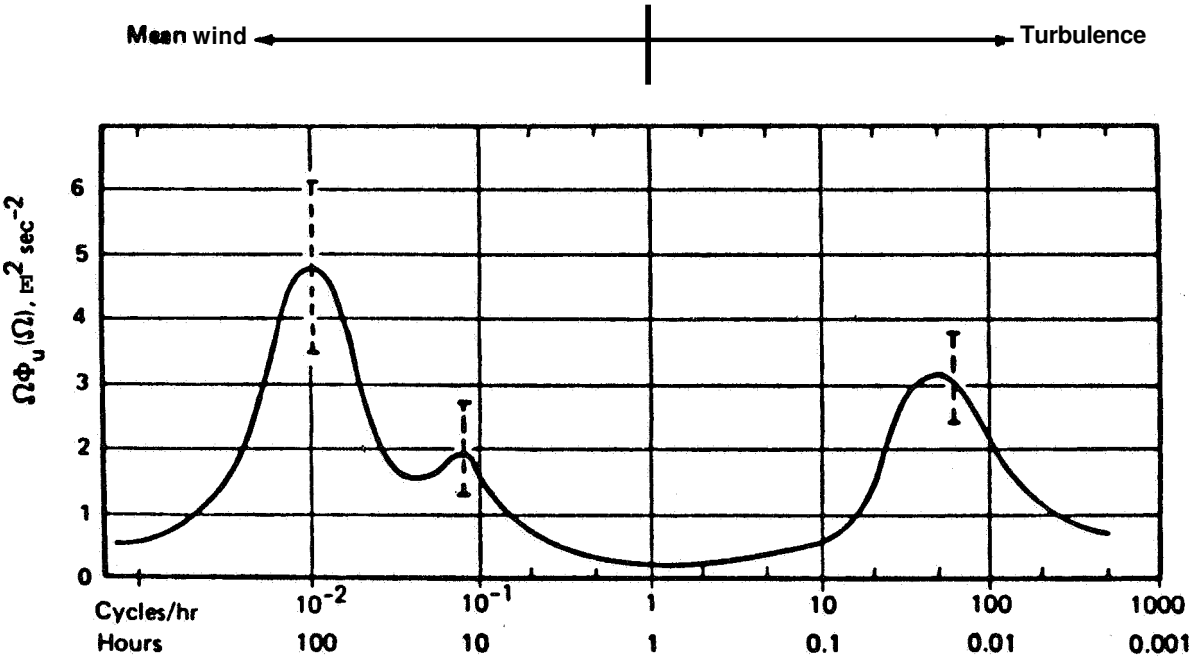

FIGURE 1 – SCHEMATICSPECTRUM OF WIND SPEED NEAR THE GROUND ESTIMATED FROM A STUDY OF VAN DER HOVEN (1957)

MEAN WIND

Analytic Description

The mean wind is characterized by:

- Zero vertical component
- Zero wind speed at the surface
- Invariant with altitude above the atmospheric boundary layer

The mean wind model having the greatest acceptance, both theoretically and empirically, is that developed from dimensional analysis. The parameters involved are:

$\frac{\partial \bar{V}_W}{\partial h}$ = mean wind shear

τ = shear stress

ρ = atmospheric density

C_P = specific heat at constant pressure

h = altitude

g = gravitational acceleration

H = heat flux

T = absolute temperature

$\frac{\partial T}{\partial h}$ = lapse rate

This inclusive list assumes:

- Pressure gradients are invariant with altitude, at least over a sufficiently constrained region.
- Viscous forces dominate pressure and Coriolis forces.
- The flow of air is fully rough so that molecular viscosity is not a significant parameter.

The parameters appear in the combinations

$$u_* = \sqrt{\frac{\tau}{\rho}} = \text{friction velocity}$$

$$\frac{kh}{u_*}\frac{\partial \bar{V}_{r,T}}{\partial h} = \text{nondimensional shear}$$

($k = 0.4$ = von Karman's constant)

$$\ell = \frac{u_*^3 C_p \rho T}{kgH}$$

Dimensional analysis then predicts

$$\frac{kh}{u_*}\frac{\partial \bar{V}_W}{\partial h} = \phi(h/\ell)$$

where $\phi(h/\ell)$ is some specific function.

It is additionally assumed that shear stress and density are invariant with altitude for a sufficiently constrained altitude region. Then

$$\bar{V}_W = \frac{u_{*_0}}{k}\int_{z_0}^{h}\frac{(h/\ell)}{h}\,dh$$

where

z_0 = the altitude at which the mean wind speed formally goes to zero

$u_{*_0} = u_*(h = 0)$

The scaling length, ℓ, is difficult to measure due to the difficulty of measuring the heat flux, so an alternate scaling length, ℓ', is introduced:

$$\ell' = \frac{u_{*_0} \; T \; \frac{\partial \bar{V}_W}{\partial h}}{kG \left[\frac{\partial T}{\partial h} + \frac{g}{C_p} \right]}$$

This alternate scaling length is equal to the dimensional analysis scaling length multiplied by the ratio of eddy conductivity to eddy viscosity and is assumed to be a constant, implying that there is a one-to-one relationship of the wind and temperature shears independent of altitude.

The alternate scaling length can be related to a more conventional and still more easily measured parameter reflecting atmospheric stability, Richardson's number:

$$R_i = \frac{\frac{g}{T}\left(\frac{\partial T}{\partial h} + \frac{g}{C_p}\right)}{\left(\frac{\partial \bar{V}_W}{\partial h}\right)^2}$$

$$\frac{h}{\ell'} = \left[\frac{\frac{g}{T}\left(\frac{\partial T}{\partial h} + \frac{g}{C_p}\right)}{\left(\frac{\partial \bar{V}_W}{\partial h}\right)^2} \right] \left(\frac{kh}{u_{*_0}} \frac{\partial \bar{V}_W}{\partial h} \right) = R_i \phi(h/\ell')$$

Richardson's number is a nondimensional ratio between the mechanical wind shear that tends to displace air and the buoyancy force, which may damp or amplify this tendency.

Richardson's number thus gives rise to the notion of atmospheric stability, a dynamic concept:

$$R_i,\ h/\ell' > 0 \rightarrow \frac{\partial T}{\partial h} > \frac{-g}{C_p}\ ;\ \text{stable (weak lapse or inversion)}$$

$$R_i,\ h/\ell' = 0 \rightarrow \frac{\partial T}{\partial h} = \frac{-g}{C_p} = -0.00536°\text{R/ft};\ \text{neutral (adiabatic lapse)}$$

$$R_i,\ h/\ell' < 0 \rightarrow \frac{T}{h} < \frac{-g}{C_p}\ ;\ \text{unstable (strong lapse)}$$

Given the nature of $\phi(h/\ell')$, the variation of R_i is known with altitude and R_i could be used in place of h/ℓ'. However, it is simpler to use h/ℓ' as it varies linearly with altitude. The greater ease involved in measuring R_i provides an indirect means of computing R.

Investigators have examined $\phi(h/\ell')$ for different regions of stability. For neutral stability $\phi(h/\ell') = 1$ and

$$\frac{\partial \bar{V}_W}{\partial h} = \frac{u_{*_0}}{kh}$$

$$\bar{V}_W = \frac{u_{*_0}}{k} \ln\left(\frac{h}{z_0}\right)$$

or, after an axis system shift to provide $\bar{V}_W = 0$ at $h = 0$,

$$\bar{V}_W = \frac{u_{*_0}}{k} \ln\left(\frac{h + z_0}{z_0}\right)$$

For neutral stability, the shear is inversely proportional to altitude and the mean wind is described by the logarithmic profile. The term z_0 reflects surface roughness and is larger for greater roughness. $z_0 = 0.15$ foot, as provided by the British specification, and is representative for autoland applications.

If the mean wind, V_{REF}, is known at some altitude, h_{REF}, the friction velocity, u_{*_0}, may be found from the equation for the mean wind profile:

$$u_{*_0} = \frac{k\bar{V}_{REF}}{\ln\left(\frac{REF + z_0}{z_0}\right)}$$

For a given wind speed at h_{REF} an increase in roughness length, z_0, is related to an increase in friction velocity, which in turn provides an increase of the shear at every altitude, a decrease in wind speed for $h < h_{REF}$, and an increase in wind speed for $h > h_{REF}$.

For near neutral stability, $\phi(h/\ell')$ may be estimated from the first two terms of a Taylor series expansion about neutral stability:

$$\phi(h/\ell') = 1 + \alpha' h/\ell' \,, \; h/\ell' << 1$$

$$a' \qquad = \text{constant}$$

Thus,

$$\bar{V}_W = \frac{u_{*_0}}{k}\left[\ln\left(\frac{h + z_0}{z_0}\right) + \alpha' h/\ell'\right]$$

which is the log-linear mean wind profile. For stable conditions ($h/\ell' > 0$), the effect of stability appears to

cause an increase in the mean wind speed and shear. Unstable conditions appear to cause a decrease in the shear and mean wind speed.

For the log-linear profile, friction velocity can be determined from the mean wind speed at a given altitude by

$$u_{*_0} = \frac{k\bar{V}_{REF}}{\ln\left(\frac{h+z_0}{z_0}\right) + \alpha' h_{REF}/\ell'}$$

Stable conditions result in a decrease and unstable conditions result in an increase of friction velocity.

Combining the effects of stability on friction velocity and the nondimensional wind shear gives

$$\frac{\bar{V}_W}{h} = \frac{\bar{V}_{REF}}{h}\left[\frac{1+\alpha' h/\ell'}{\ln\left(\frac{h_{REF}+z_0}{z_0}\right) + \alpha' h_{REF}/\ell'}\right]$$

Stable conditions cause the shear to be greater than for neutral conditions above some altitude, but less than the neutral stability shear below that altitude. The reverse is true for unstable conditions.

For near neutral stability, the constant ℓ' can be determined by knowing Richardson's number at some altitude, h_{REF}:

$$h/\ell' = R_i\phi(h/\ell') = R_i(1+\alpha' h/\ell'), h/\ell' << 1$$

$$1/\ell' = \frac{R_{i_{REF}}}{h_{REF}(1 - R_{i_{REF}})} \cong \frac{R_{i_{REF}}}{h_{REF}}$$

The general form of the mean wind profile may be reformulated to represent the contribution of neutral conditions plus the increment due to nonneutral conditions:

$$\bar{V}_W = \frac{u_{*0}}{k}\left[\ln\left(\frac{h+z_0}{z_0}\right) + f(h/\ell')\right]$$

where

$$f(h/\ell') = \int_0^h \frac{\phi(\xi) - 1}{\xi}\, d\xi$$

Different investigators have developed expressions for the mean wind shear for various regions of stability. For unstable conditions:

$$\phi(h/\ell') = \frac{1}{1 - \beta' R_i}^{1/2}, \quad \text{small negative } R_i$$

$$\beta' = \text{constant}$$

$$\frac{\partial \bar{V}_W}{\partial h} \sim h^{-4/3}, \quad \text{strong instability}$$

A form that matches the logarithmic, log-linear, and the above two expressions is the KEYPS equation:

$$\phi(h/\ell') = \frac{1}{(1 - \gamma' R_i)^{1/4}} \quad R_i \leq 0$$

$$\gamma' = 2\beta' = 4\alpha' = \text{constant}$$

This form has been adopted along with $\gamma' = 18$, which implies $\alpha' = 4.5$, values in good agreement with measurements. The

corresponding relationship between nondimensional altitude and Richardson's number is

$$h/\ell' = \frac{R_i}{(1 - \gamma' R_i)^{1/4}}$$

An explicit expression for the mean wind shear and, consequently, the mean wind speed in terms of h/ℓ' cannot be found, but such a relationship can be determined numerically.

For stable conditions, the log-linear relationship has been found to hold for surprisingly large values of h/ℓ'; for very stable conditions, knowledge is poor. The best expression found for very stable conditions is

$$\phi(h/\ell') = (1 + \alpha')$$

which once again results in a shear inversely proportional to altitude. The corresponding mean wind profile is

$$\bar{V}_W = \frac{u_{*0}}{k} \left\{ \ln \left(\frac{h + z_0}{z_0} \right) + \alpha' \left| 1 + \ln(h/\ell') \right| \right\} \qquad \ell' > 1$$

For $h/\ell' > 1$, Richardson's number and nondimensional altitude are related by

$$h/\ell' = (1 + \alpha') R_i$$

Combining the descriptions of $\phi(h/\ell')$ adopted provides the nondimensional shear as a function of h/ℓ', as shown in Figure 2. The corresponding function $f(h/\ell')$ for the mean wind equation is **shown** in Figure **3.** The combined relationships between h/ℓ' and R_i are shown in Figure *4.*

The wind above the edge of the boundary layer (geostrophic wind) is that which remains invariant with

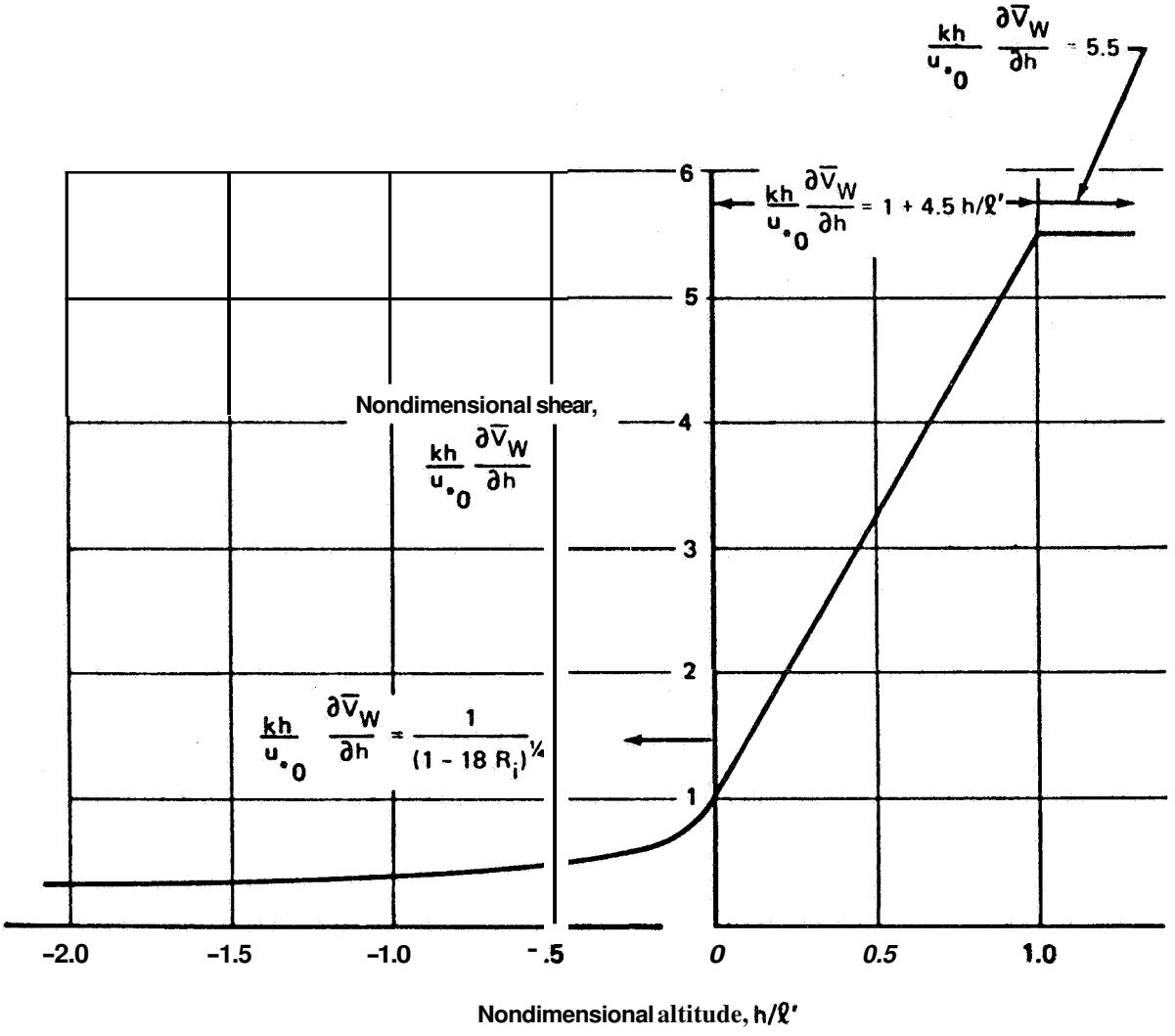

FIGURE 2.– SELECTED NONDIMENSIONAL SHEAR DESCRIPTION

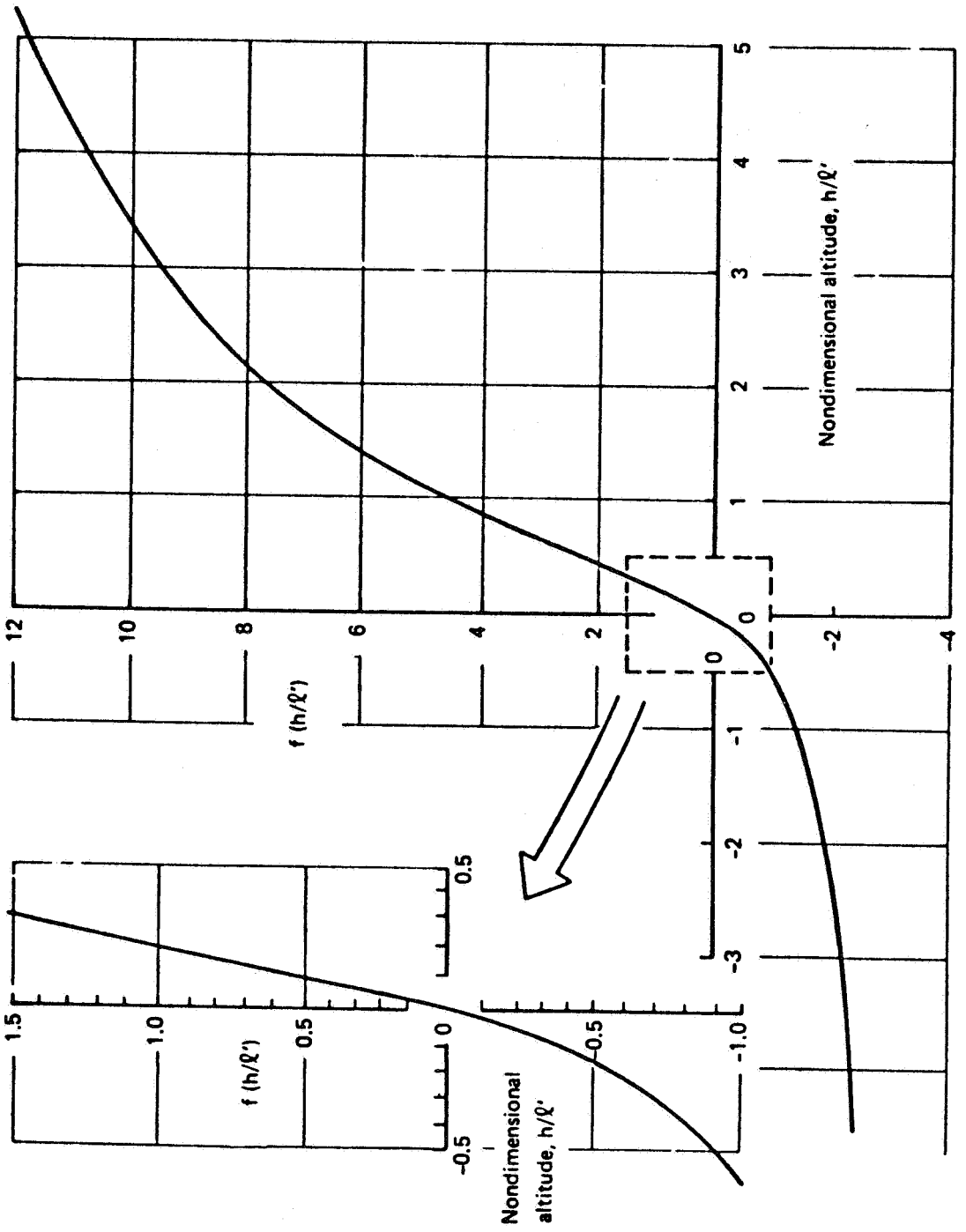

FIGURE 3 -CONTRIBUTION OF NON-NEUTRAL STABILITY TO MEAN WIND

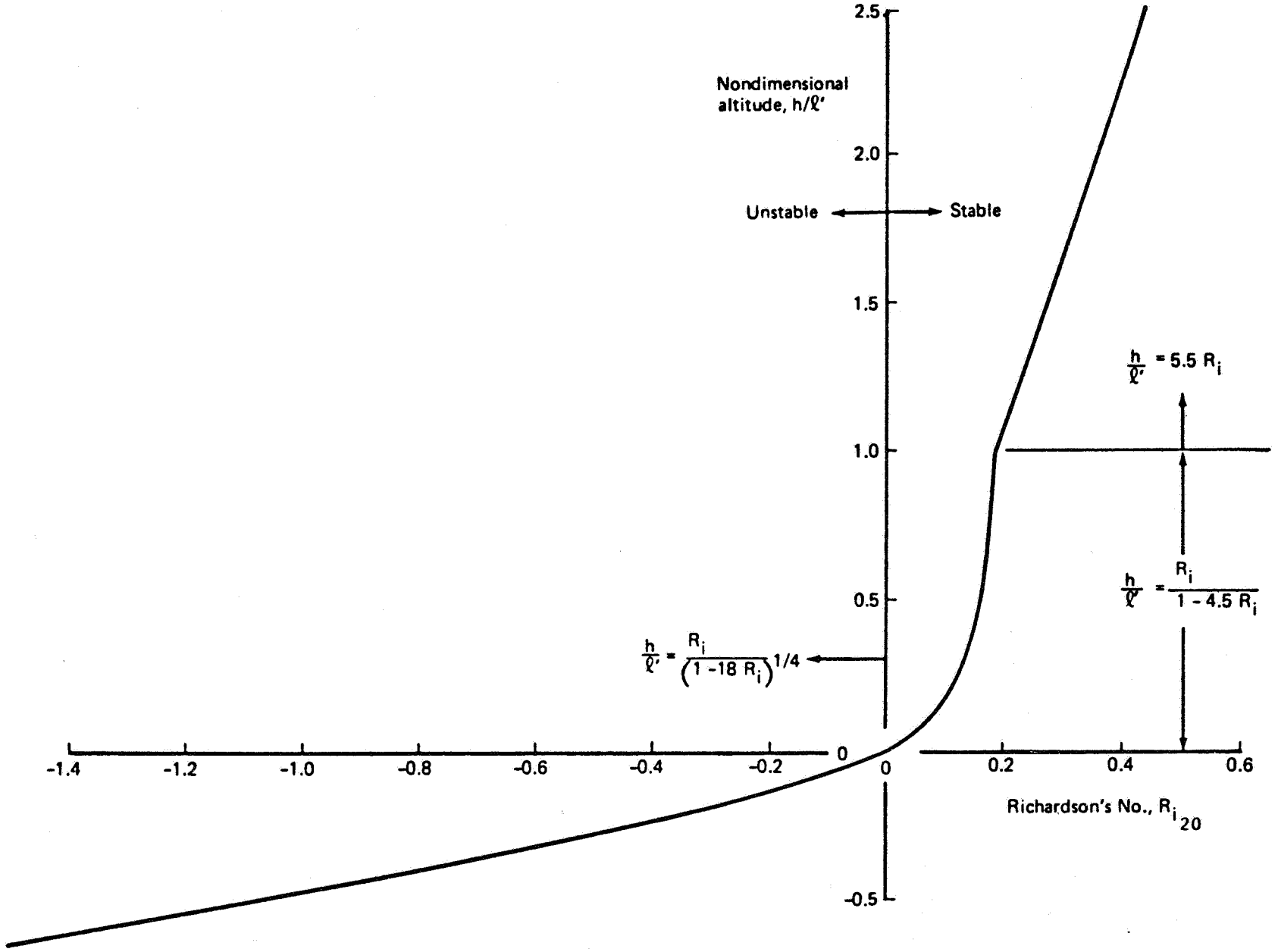

FIGURE — LOW ALTITUDE RICHARDSON'S NUMBER PROFILE

surface conditions and atmospheric stability in the boundary layer. There are little data on geostrophic winds, and relationships between winds near the surface and above the boundary layer are poor. Rather than relating low-altitude wind conditions to the geostrophic wind, the wind profile is extrapolated from low-altitude winds. The American standard for airport wind measurement is 20 feet. The extrapolation of winds and shears based on wind speeds at 20 feet is performed through the determination of friction velocity:

$$u_{*_0}/k = \frac{V_{20}}{\ln\left(\frac{20.15}{0.15}\right) + f(h_{RE}/\ell')} \quad \text{(Fig. 5)}$$

Figure 5 shows friction velocity to continually decrease for increasing stability. The nondimensional shear, Figure 2, is constant for $h/\ell' > 1$. Thus, the shear, given by

$$\frac{\partial \bar{V}_W}{\partial h} = \frac{\bar{V}_{20}}{h}\left(\frac{u_{*_0}/k}{\bar{V}_{20}}\right)\left(\frac{kh}{u_{*_0}}\frac{\partial \bar{V}_W}{\partial h}\right)$$

must decrease for $h/\ell' > 1$.

The scaling length, ℓ', may be determined for Richardson's number measured at another altitude different from 20 feet, but since the choice appears arbitrary, $1/\ell'$ is determined from Figure *4* for Richardson's number measured at 20 feet. The description provided thus far still suffers from a restriction: the dimensional analysis descriptions are valid only over the altitude region for which shear stress differs insignificantly from that at the surface. Insignificant variations of the shear stress have been variously estimated to occur up to 65 to 650 feet, significantly less than the objective of 1000 feet. At progressively

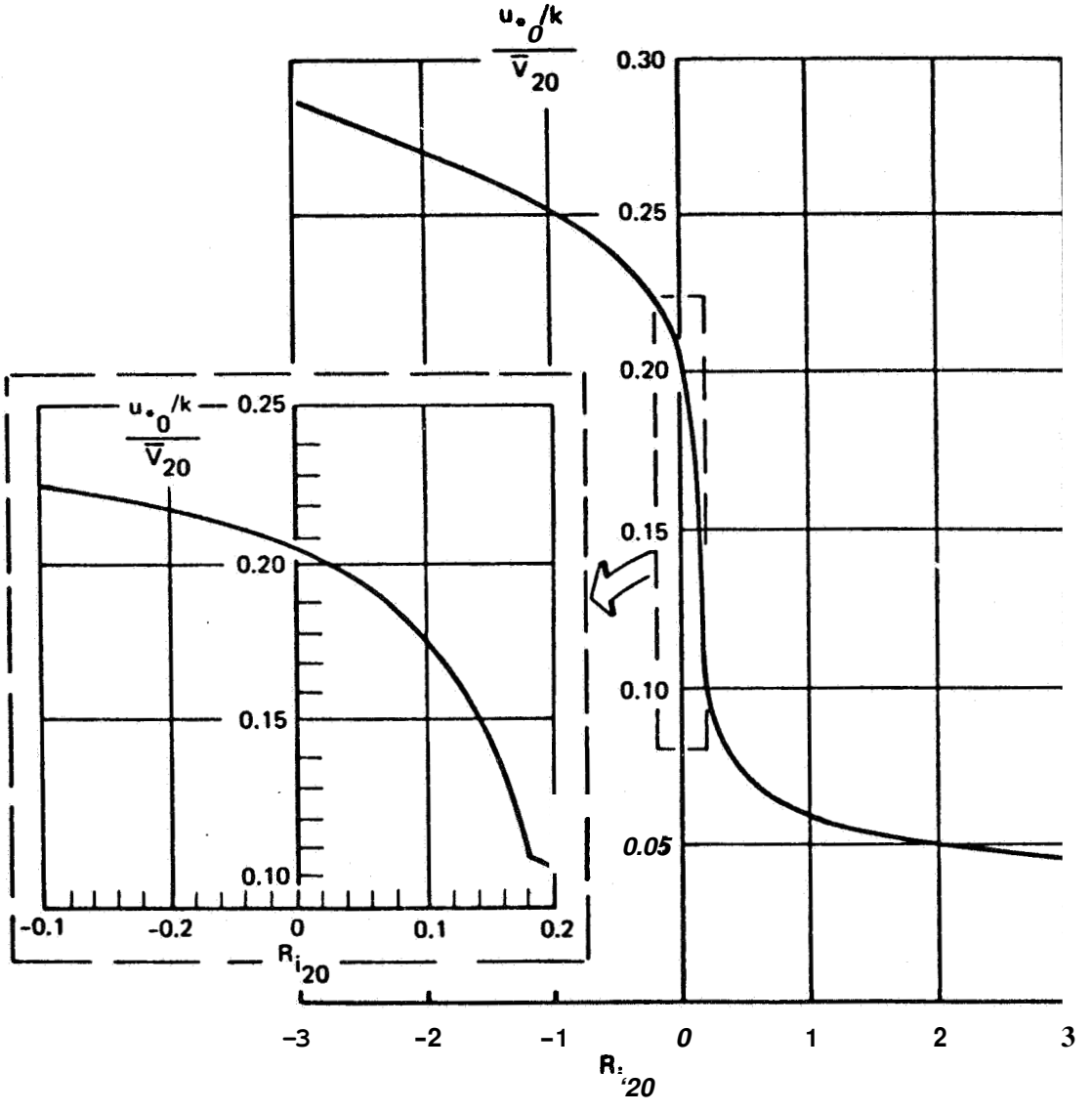

FIGURE 5 – MEAN WIND PROPORTIONALITY CONSTANT

higher altitudes, a progressively greater overestimation of the mean wind speed and shear occur; the description of the mean wind never does provide a constant mean wind with altitude above the boundary layer. A mechanism for adjusting the description has been found through descriptions of shear stress (friction velocity) variations throughout the boundary layer.

By expanding shear stress with altitude about conditions at the boundary layer (where shear stress is zero) using a Taylor series, expressions for friction velocity variations with altitude and for the boundary layer depth, d, are developed:

$$u_* = u_{*_0}(1 - h/d)$$

$$d = u_{*_0}/5.35\ f$$

where

f = Coriolis parameter

$= 2\omega_E \sin \lambda$

ω_E = angular velocity of the earth

A = latitude

Most of the United States and a majority of the world airport activity lies between 30" and 50" latitude, so a fixed latitude, $A = 40°$, is adopted for determining the boundary layer depth. Then,

$$d = 2000\ u_{*_0}$$

To incorporate the shear stress variation into the mean wind description, the assumption that the shear is

proportional to friction velocity at the surface is dropped, and it is assumed that the shear is proportional to the local level of friction velocity. Then,

$$\frac{\partial \bar{V}_W}{\partial h} = \frac{u_*}{kh}\,\phi(h/\ell') = \left(\frac{u_*}{u_{*_0}}\right)\frac{u_{*_0}}{kh}\left(\frac{kh}{u_*}\,\frac{\partial \bar{V}_W}{\partial h}\right)$$

$$= \left(1 - \frac{h}{d}\right)\frac{\bar{V}_{20}}{h}\left(\frac{u_{*_0}/k}{\bar{V}_{20}}\right)\left(\frac{kh}{u_*}\,\frac{\partial \bar{V}_W}{\partial h}\right)$$

The shear now smoothly decreases to zero at the edge of the boundary layer with increasing altitude. Near the surface, where $h/d \cong 0$, the constant shear stress model is unaffected.

The corresponding expression for the mean wind speed is

$$\bar{V}_W = \bar{V}_{20}\left(\frac{u_{*_0}/k}{\bar{V}_{20}}\right)\left[\ln\left(\frac{h+z_0}{z_0}\right) + f(h/\ell') - \frac{h}{d}\,g(h/\ell')\right]$$

The function, $g(h/\ell')$, (Fig. 6) is derived from $f(h/\ell')$. It is always positive, is equal to one for neutral stability, and increases with increasing stability.

Probabilistic Description

The additional parameters required to complete the description of the mean wind speed and mean wind shear are specifications for wind speed and Richardson's number at a 20-foot altitude.

Based on Weather Service reports at U.S. airports, a description of airport wind speeds has been developed that describes 10-minute averages measured each hour for 10 years. The data were taken prior to establishing 20 feet as a standard anemometer height, so anemometer heights varied

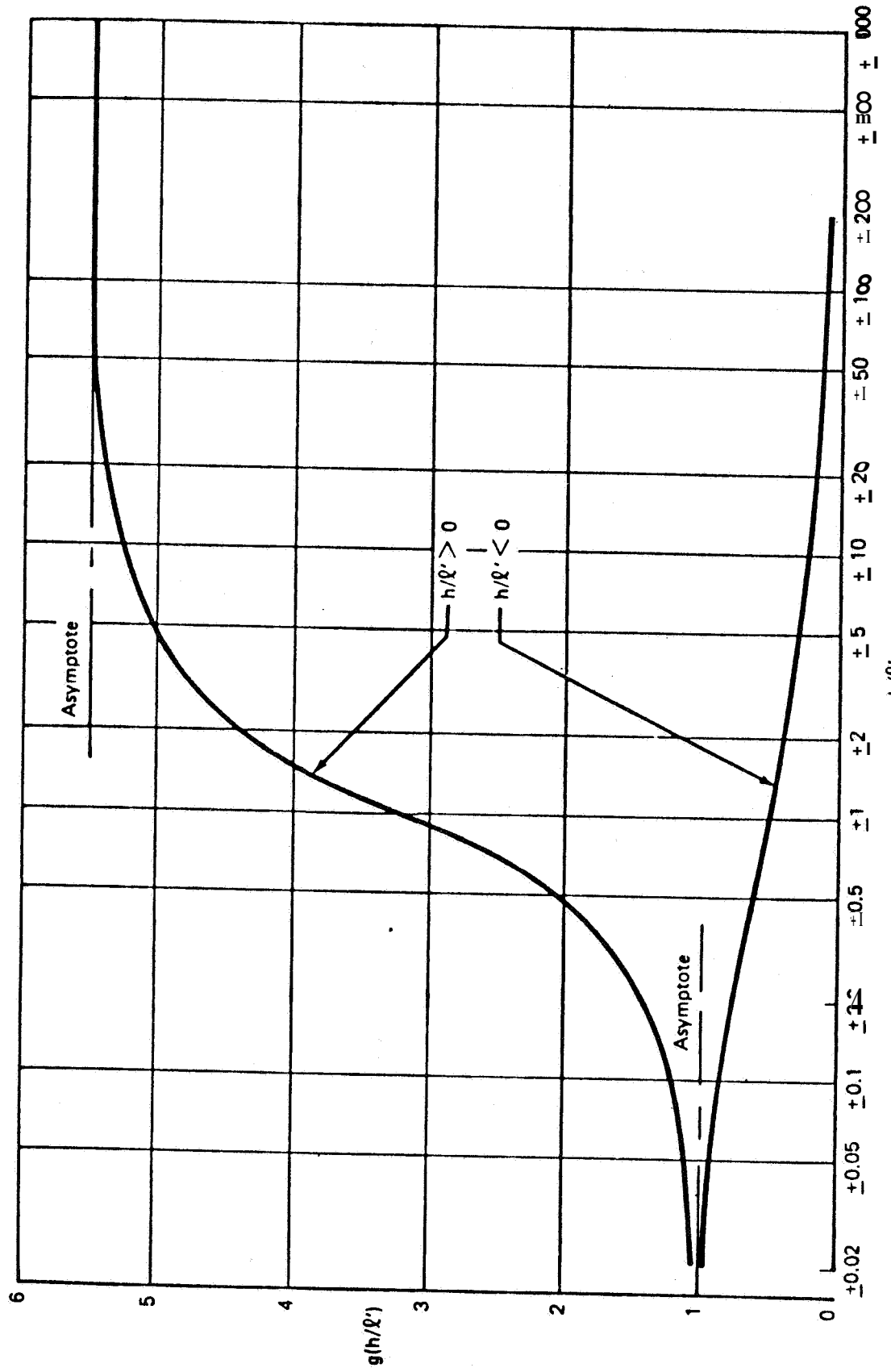

FIGURE 6 – VARIABLE SHEAR STRESS CORRECTION TO WIND PROFILE

widely from airport to airport. From data for 132 U.S. airports, data were selected from 24 sites where anemometer heights varied from 20 to 35 feet with an average height of about 26 feet. The remaining sites have anemometers located from above 35 to 120 feet above the ground and were considered to be too high to represent wind speeds at 20 feet. In developing a composite description for all 24 airports, the distributions from each site were weighted equally. The resulting descriptions, Figure 7, provide for 8 knots exceeded 50% of the time and 22.7 knots exceeded 1% of the time. For 39 of the same 132 sites, data for the wind speed distribution when visibility was less than 0.5 mile (prepared by the Weather and Flight Service Station Branch of the FAA) are presented. For low visibility, wind speeds are much lower than for clear conditions; for low visibility, 4.5 knots is exceeded 50% of the time and 14 knots is exceeded 1% of the time.

From the data for the 24 U.S. airports, distribution of wind components along and across runways was developed, assuming the runway is aligned to the prevailing wind. Crosswinds from the left and right were found to be equally likely. The distribution of crosswind magnitude, Figure 8, provides for exceeding a 5-knot crosswind 50% of the time and a 19-knot crosswind 1% of the time. When the distribution of crosswinds is plotted for both positive and negative crosswinds, the distribution is closely Gaussian (standard deviation equal to 6.5 knots), with deviations from a Gaussian distribution occurring in the tails (1.65 standard deviations from zero crosswind).

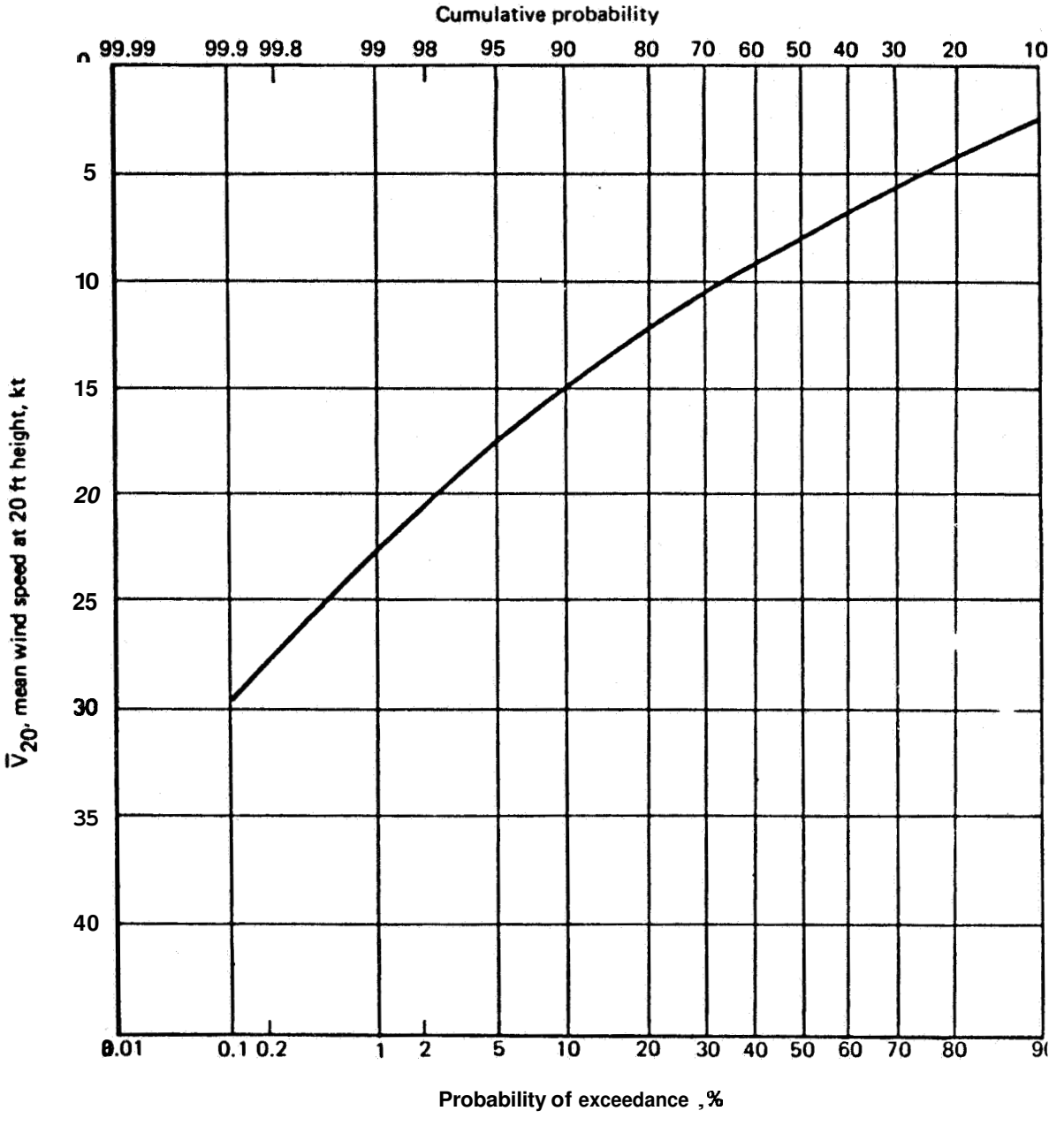

FIGURE 7 – MEAN WIND CUMULATIVE/EXCEEDANCE PROBABILITY

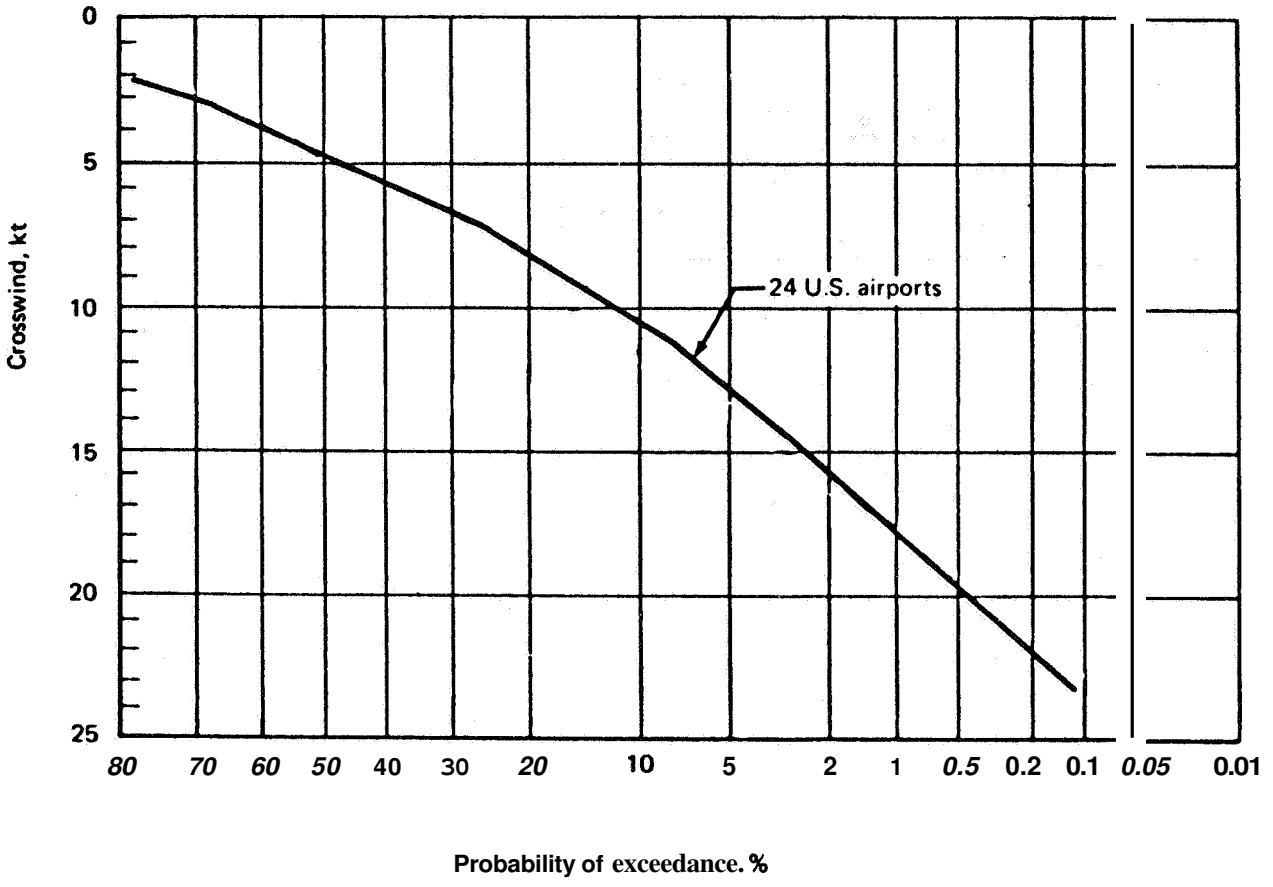

FIGURE a –TOTAL CROSSWIND INFORMATION COMPILED FROM 24 US. AIRPORTS

The distribution of down runway components is also closely Gaussian (Fig. 9) with a mean and standard deviation of 1 and 7 knots, respectively. The probability of a wind component in the direction of the prevailing wind is 59%. The distribution for the magnitude of the component of mean wind aligned to the runway (Fig. 10) provides for 5 knots exceeded 50% of the time and 19 knots exceeded 1% of the time.

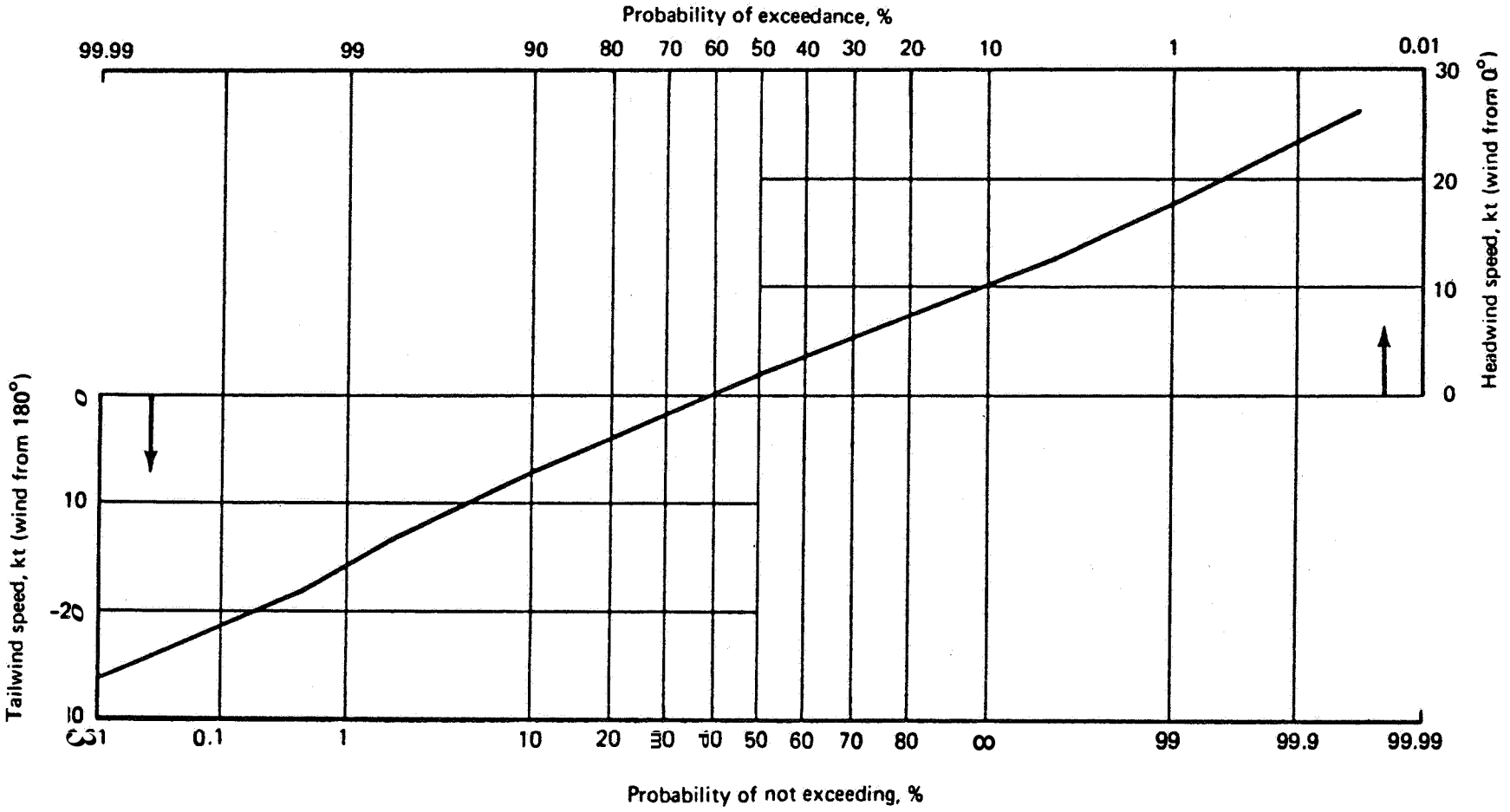

FIGURE 9 – HEADWIND–TAILWIND DESCRIPTION COMPILED FROM 24 U.S. AIRPORTS

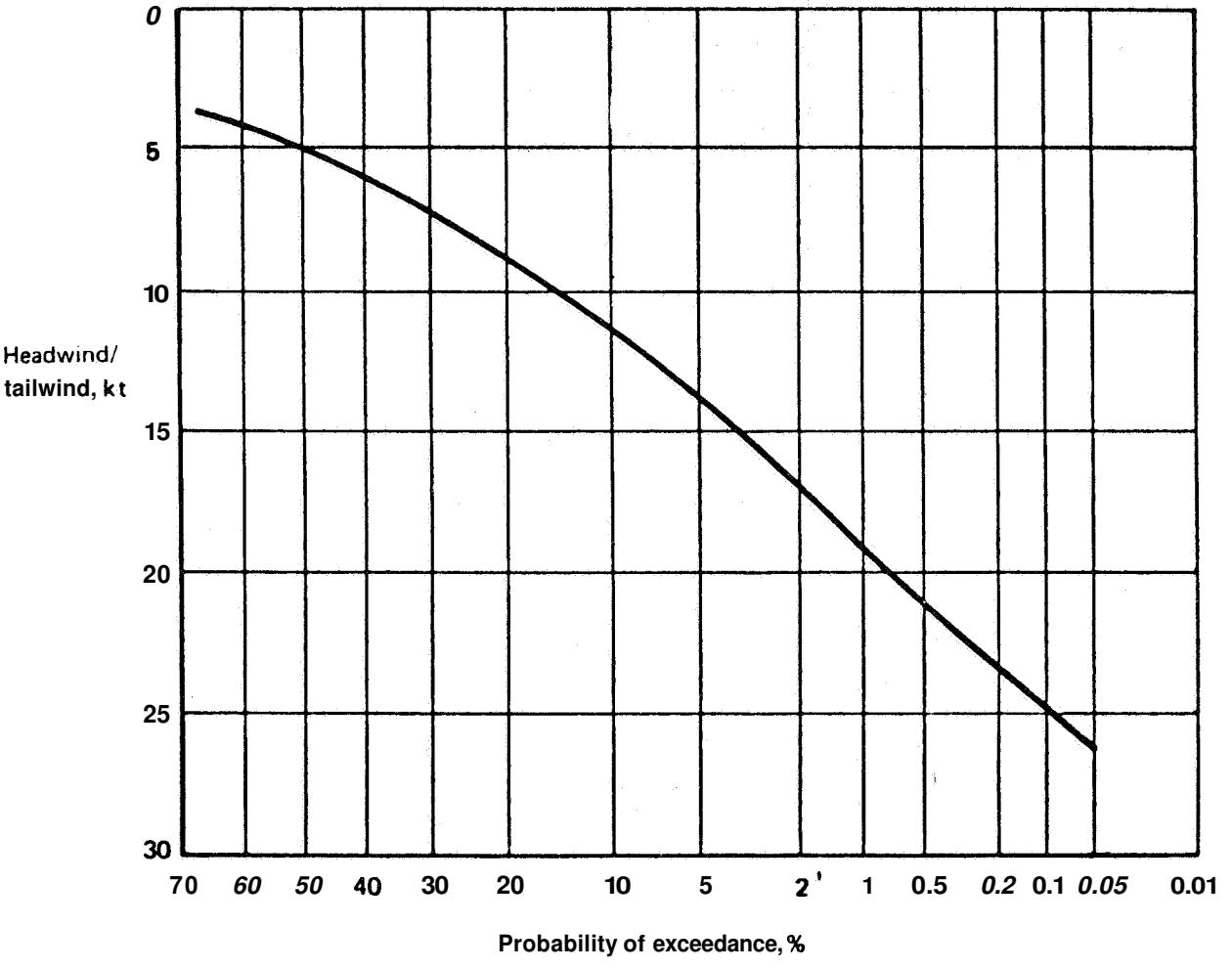

FIGURE 10 – TOTAL HEADWIND–TAILWIND MEAN OF 24 U.S. AIRPORTS

Distribution of mean wind shears was also investigated. Distributions were much broader near the surface than at higher altitudes, conforming to the analytic description. The introduction of atmospheric stability into the mean wind description in such a way that wind shears increase with increasing stability (up to a point), as well as with wind speed and the finding that atmospheric stability is inversely related to wind speed, introduce confusion as to whether maximum shears occur at high wind speeds where stability is close to neutral or at low wind speeds where stability is high. Data from the literature show the greatest shears occur at the most stable lapse rates and at low wind speeds (both average and maximum wing shears decrease monotonically with increasing wind speeds at high wind speeds), conflicting with commonly employed wind models that assume neutral stability and increasing shears with wind speed, thus emphasizing the importance of atmospheric stability as a mean wind parameter.

The literature was not productive for describing distributions of atmospheric stability, so probability distributions were generated by reducing data from towers located at Cedar Hills, Texas, and Cape Kennedy, Florida. The distributions for the two sites differed substantially (Fig. 11), with the Cedar Hills data being more stable. Evaluation of the climatology and wind characteristics of the two sites led to the conclusion that the Cape Kennedy stability data were more representative of average airport conditions. Consequently, the Cape Kennedy data were selected for use with the model. Although the Cape Kennedy data reflected the lesser stability, over 70% of the cases at the site were stable (versus 90% of the cases at Cedar Hills).

The strong interdependence between the distribution of atmospheric stability and near-surface wind speed can be seen

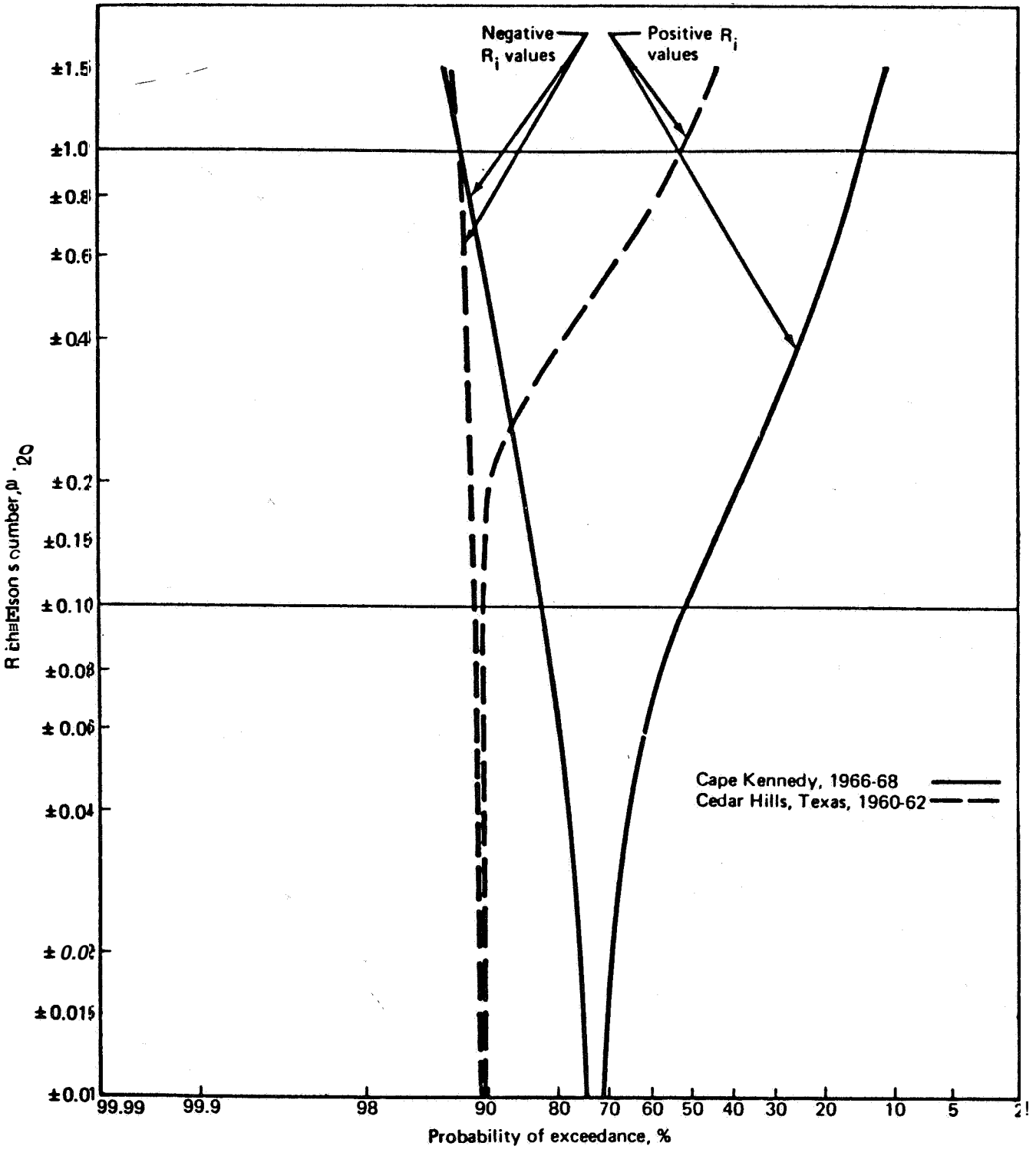

FIGURE 11 – PROBABILITY OF EXCEEDANCE OF R_i FOR ALL WIND SPEEDS

in Figure 12. Although the atmospheric stability distribution narrows substantially about neutral conditions at increasing wind speeds, the distribution remains significantly broad at high wind speeds. The data in Figure 12 were faired and extrapolated to account for the relatively small data sample (one site for three years with near-calm wind speed conditions excluded) and have been cross plotted at constant 20-foot-altitude wind speeds in Figures 13, 14, and 15.

The mean wind speed and atmospheric stability distribution curves may be used by (1) defining wind speed/stability regions and assigning average values of wind speed and Richardson's number to each region; (2) by simulating the aircraft for each wind speed/Richardson's number combination; and (3) by combining the results of the simulation according to the joint; probabilities of each region. Alternately, the simulation may be used to define random combinations of mean wind speed and Richardson's number. A random number generator, providing a uniform distribution between zero and one, is used to determine two random numbers. A mean wind speed at an exceedance probability equal to one of the random number generators is found. The Richardson's number associated with the exceedance probability for the mean wind speed determined equal to the second random number is found. The Richardson's number and mean wind speed then determine the mean wind speed and shear profiles. When this process is repeated, the joint distribution of wind speed and Richardson's number is reproduced.

Application to Aerodynamics

In order to determine the aerodynamic forces and moments, the mean wind must be resolved into body axis components, an axis system attached to the airplane. The

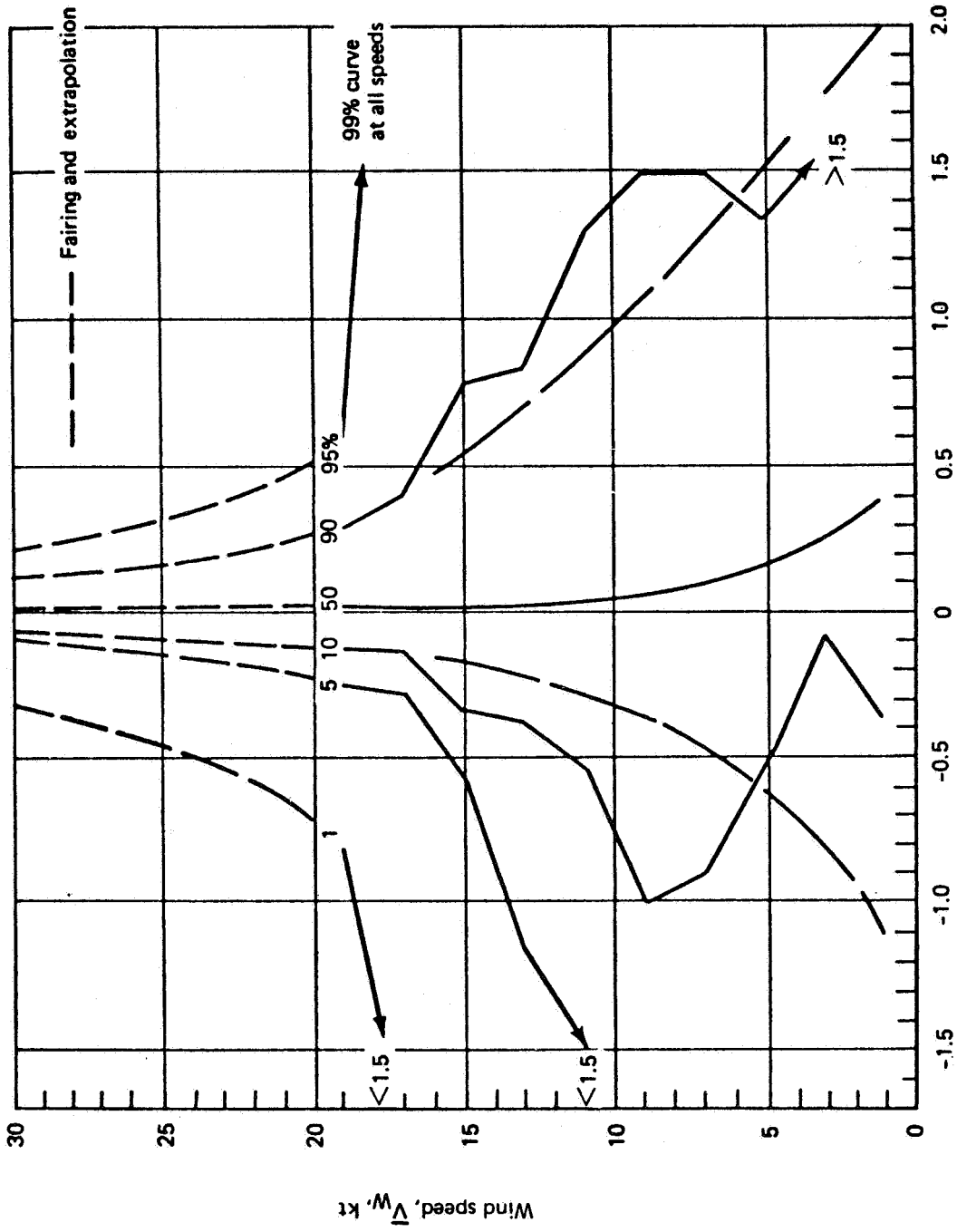

FIGURE 12 – PERCENT FREQUENCY OF OCCURRENCE, WIND SPEED VS R_i, CAPE KENNEDY, 1966-68

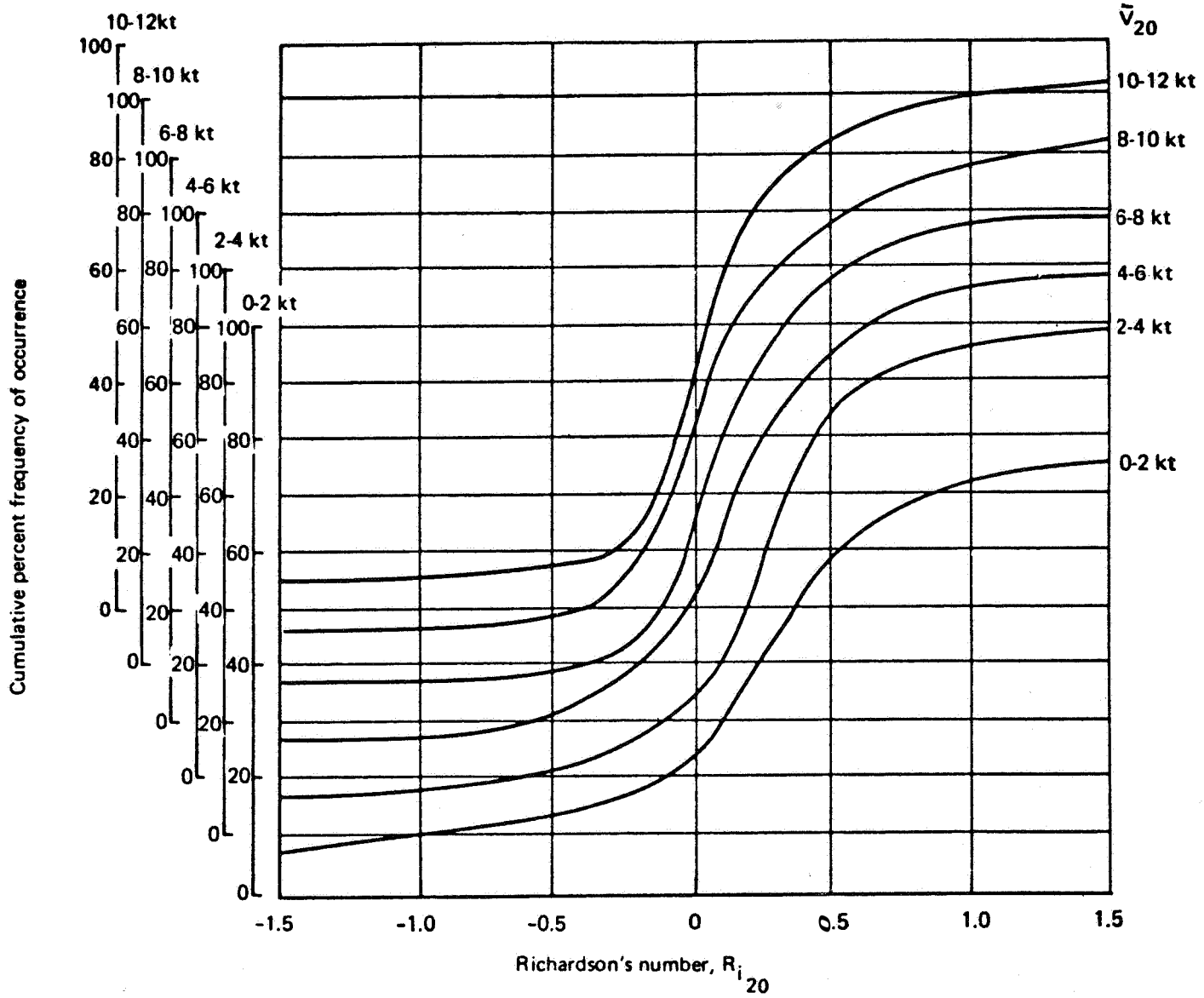

FIGURE 13 – CUMULATIVE PERCENT FREQUENCY OF OCCURRENCE OF R_i AT GIVEN WIND SPEEDS, 0 TO 12 KNOTS

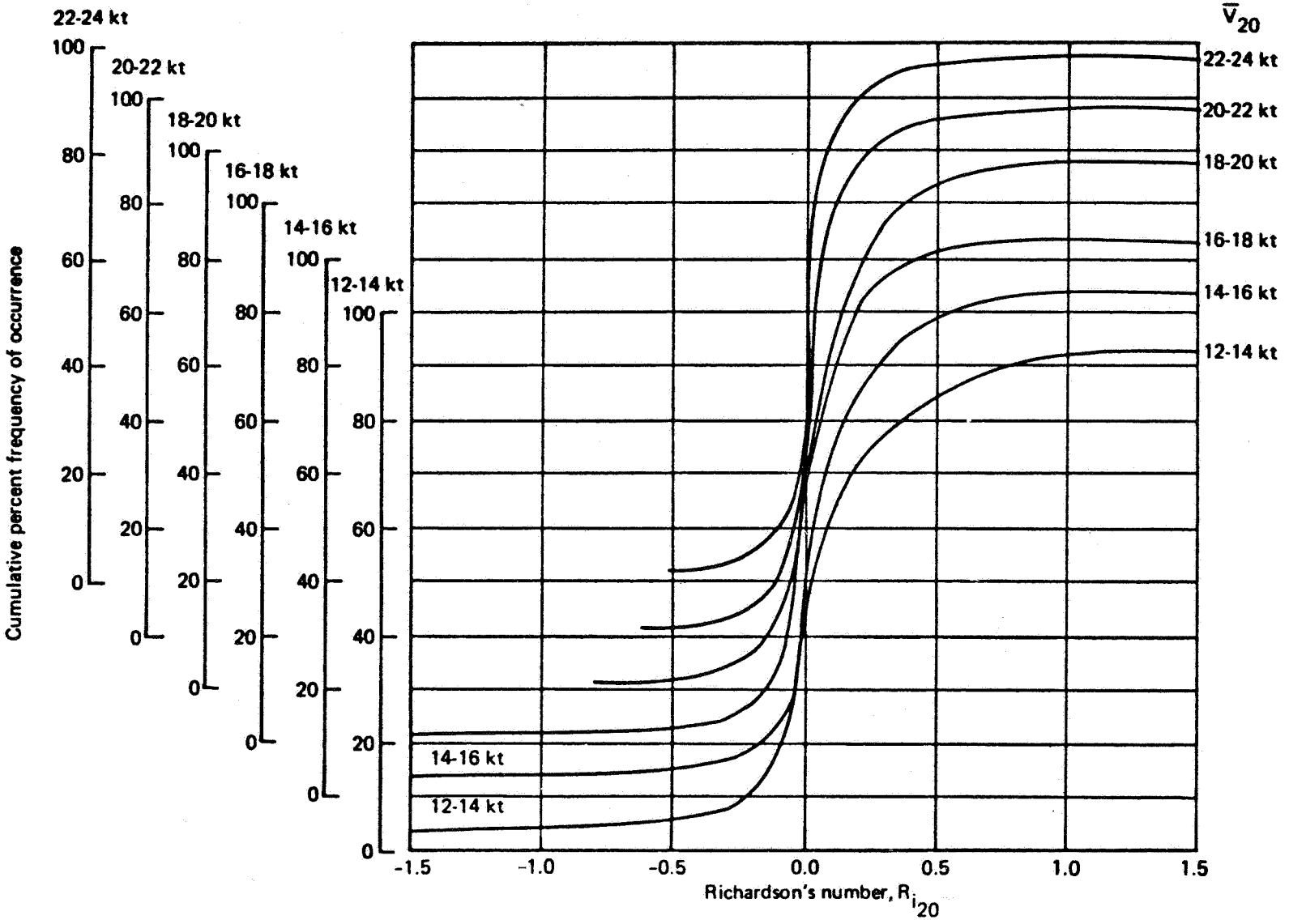

FIGURE 10 – CUMULATIVE PERCENT FREQUENCY OF OCCURRENCE OF R_i AT GIVEN WIND SPEEDS, 12 TO 24 KNOTS

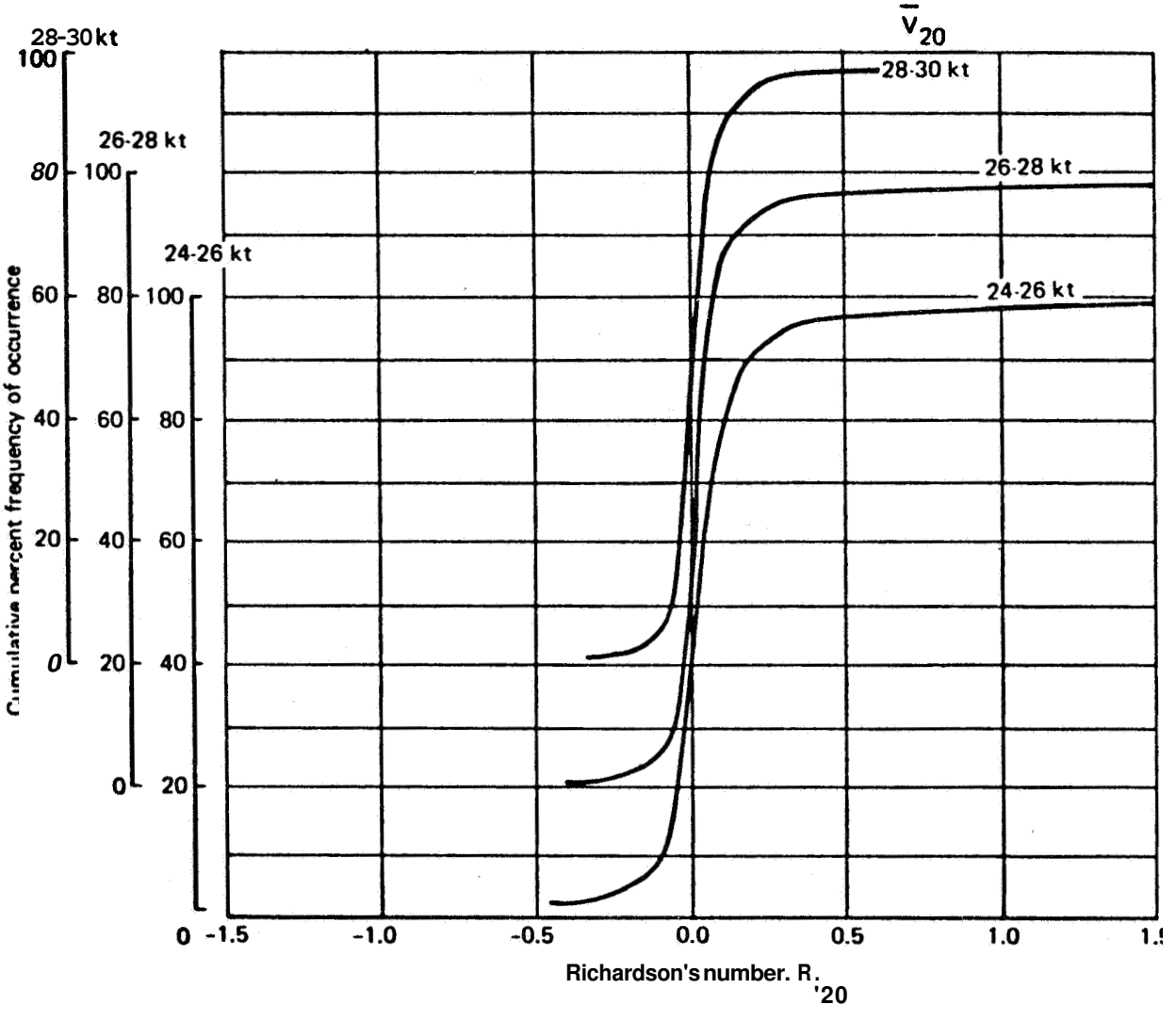

FIGURE 15 – CUMULATIVE PERCENT FREQUENCY OF OCCURRENCE OF R_i AT GIVEN WIND SPEEDS, 24 TO 30 KNOTS

transformation required is presented in Figure 16 and depends on the orientation of the airplane's body axis with respect to the wind, defined by the Euler yaw, pitch, and roll angles and the direction to which the wind is blowing (negative of conventional wind heading). The introduction of wind heading presents an additional mean wind parameter that must be known at each altitude. A variation of wind heading with altitude (heading shear) has an effect on the shear that the airplane sees that is added to the mean wind speed shear effect.

Analytic descriptions for the variation of wind heading with altitude have been investigated, but these descriptions lack empirical support. A small amount of heading shear probability distribution data was found in the literature. The data indicate a majority of heading shears are within ±3°/100 feet and a greater tendency to rotate counter-clockwise while approaching the surface. The tower data used to determine the atmospheric stability distribution were also evaluated for heading shear information. Distributions tended to be larger near the surface but constant above about 150 feet. No consistent trend of the profile shapes could be found. Heading shear was found to be uncorrelated with both wind speed and atmospheric stability. In order for the heading shear to be significant, the wind speed must also be large (body axis shear components involve the combination $\bar{V}_W \, d\bar{\psi}_W/dh$ only). The probability of having a large heading shear and wind speed shear is sufficiently remote and the information for specifying the variation of wind heading with altitude is sufficiently poor so that a representation of wind heading dependence upon altitude is not attempted; the wind heading is assumed to remain constant and equal to that at the surface. The distribution of wind

BODY AXIS MEAN WIND COMPONENTS

$$\begin{Bmatrix} \bar{u}_W \\ \bar{v}_W \\ \bar{w}_W \end{Bmatrix} = \begin{Bmatrix} \cos(\psi - \bar{\psi}_W)\cos\theta \\ \cos(\psi - \bar{\psi}_W)\sin\theta\sin\phi \\ -\sin(\psi - \bar{\psi}_W)\cos\phi \\ \cos(\psi - \bar{\psi}_W)\sin\theta\cos\phi \\ +\sin(\psi - \bar{\psi}_W)\sin\phi \end{Bmatrix} \bar{V}_W$$

BODY AXIS MEAN WIND SHEAR COMPONENTS

$$\begin{Bmatrix} \frac{\partial \bar{u}_W}{\partial h} \\ \frac{\partial \bar{v}_W}{\partial h} \\ \frac{\partial \bar{w}_W}{\partial h} \end{Bmatrix} \cdot \begin{matrix} \cos(\psi - \bar{\psi}_W)\cos 0 \\ \cos(\psi - \bar{\psi}_W)\sin\theta\sin\phi \\ -\sin(\psi - \bar{\psi}_W)\cos\phi \\ \cos(\psi - \bar{\psi}_W)\sin\ \cos \\ +\sin(\psi - \bar{\psi}_W)\sin\phi \end{matrix} \frac{d\bar{V}_W}{dh}$$

BODY AXIS TURBULENCE COMPONENTS

$$u_{A_P} = \left[\cos\alpha\cos\beta\cos\theta + \sin\beta\sin\theta\sin\phi + \sin\alpha\cos\beta\sin\theta\cos\phi\right] V^{A}{}_{CG}$$

$$v_{A_P} = \left[\sin\beta\cos\phi - \sin\alpha\cos\beta\sin\phi\right] v_{A_{CG}}$$

$$\Delta\psi = -\tan^{-1}\frac{v_{A_{TG}}}{u_{A_{TG}}} \cong -\beta$$

$$\begin{Bmatrix} u_T \\ v_T \\ w_T \end{Bmatrix} = \begin{bmatrix} \cos\Delta\psi\cos\theta & \sin\Delta\psi\cos\theta & -\sin\theta \\ \cos\Delta\psi\sin\theta\sin\phi - \sin\Delta\psi\cos\phi & \sin\Delta\psi\sin 0\sin\phi + \cos\Delta\psi\cos\phi & \cos\theta\sin\phi \\ \cos\Delta\psi\sin\theta\cos\phi + \sin\Delta\psi\sin\phi & \sin\Delta\psi\sin 0\cos\phi - \cos\Delta\psi\,sing & \cos\theta\cos\phi \end{bmatrix} \begin{Bmatrix} u_{T_{TG}} \\ v_{T_{TG}} \\ w_{T_{TG}} \end{Bmatrix}$$

FIGURE 16 – *TRANSFORMATIONS*

heading at the surface was developed from wind roses for the same 24 sites used to determine the wind speed distribution and is presented in Figure 17.

A major factor to which longitudinal touchdown dispersions are attributed is the longitudinal wind shear component. Considerable literature has been written on the subject, but conflicting conclusions are provided. Some predict a headwind shear will cause an overshoot, while others predict an undershoot. Some of the differences of opinion can be attributed to different trim and operation procedures. However, it is concluded that one of two airplanes can overshoot while the other undershoots due to a wind shear, even if both are operated in the same manner.

The effect of a steady wind is to alter the pitch attitude (θ) at which to trim to hold a given glideslope (γ):

$$\theta \cong \left[1 + \frac{\bar{V}_W \cos(\psi - \bar{\psi}_W)}{V_A} \right] \gamma + \alpha$$

where $\bar{\psi}_W = 0$ is a tailwind. For a headwind and a negative glideslope, the pitch attitude must be increased by $(\bar{V}_W/V_A)\gamma$ from that for still air and the thrust increased by $\Delta(\text{thrust}) = W\Delta\theta$, or the airplane will touch down short.

If the airplane is trimmed for a headwind at a high altitude and the headwind decreases with altitude, the pitch attitude must be decreased throughout the approach and thrust correspondingly decreased, or else the airplane will touch down long due to the attitude effect.

There is also a second effect of a wind shear. If the approach is to be performed at constant airspeed, changes in the wind speed must be matched with changes in the inertial speed. To provide inertial acceleration, thrust must be changed by

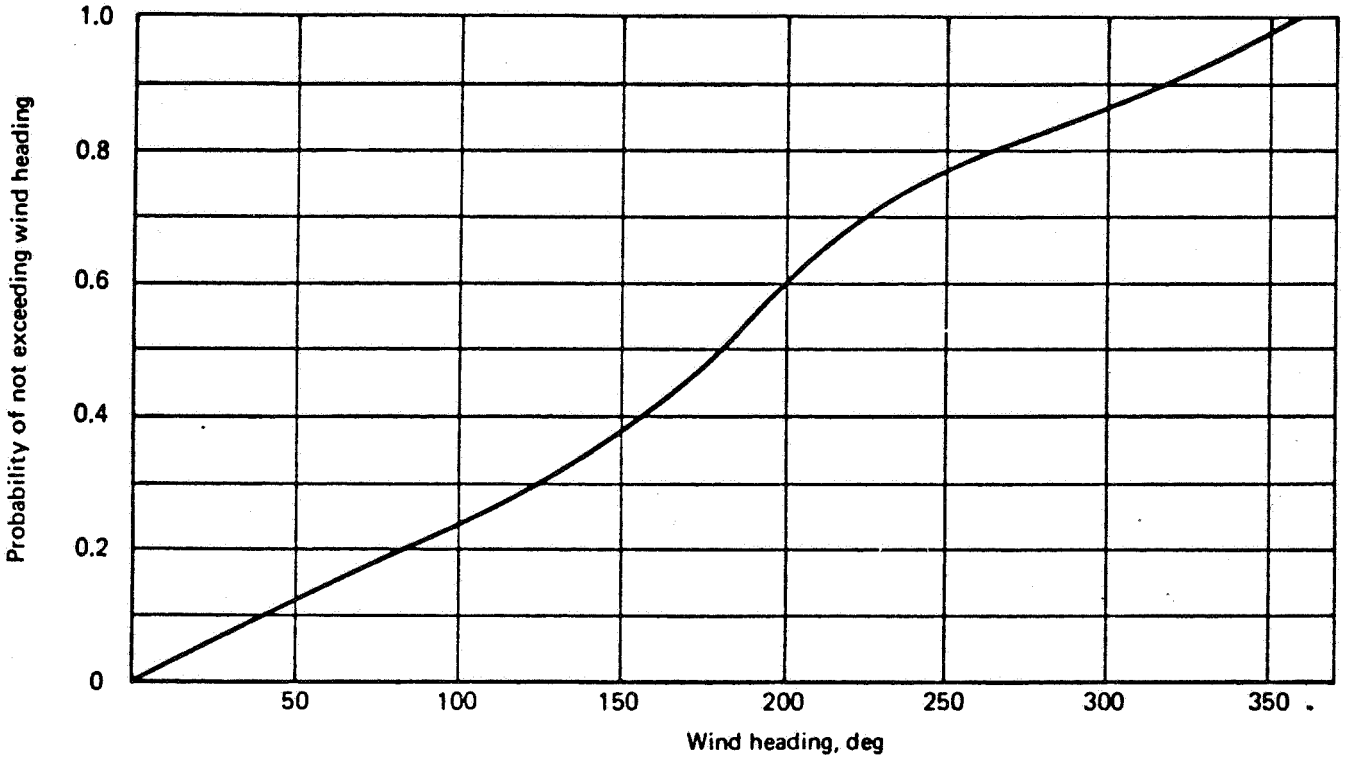

FIGURE 17 – WIND HEADING CUMULATIVE PROBABILITY MODEL

$$\Delta(\text{thrust}) \cong \frac{W(V_A + \bar{V}_W)}{g} \frac{d\bar{V}_W}{dh} \gamma$$

For a headwind that diminishes during an approach

$$\frac{d\bar{V}_W}{dh} \gamma > 0$$

and thrust must be increased or the touchdown will be short.

The combination of the attitude and acceleration effects is

$$\frac{AT}{W} \cong \gamma \frac{\Delta V_W}{V_A} + \frac{(\bar{V}_A + \bar{V}_W)}{g} \frac{d\bar{V}_W}{dh}$$

So long as the magnitude of the wind increases with altitude and the airplane is trimmed for the high attitude wind, the two terms have opposite signs. For airplanes with low airspeeds, the attitude effect tends to dominate. For a given airplane, the acceleration effect will be stronger at lower altitudes where the shear is relatively strong compared to the total change of wind speed. This evaluation presumes the airplane is controlled in an open-loop manner. The ability to attain closed-loop control, either by the pilot or the autoland system, depends in part upon the open-loop stability of the aircraft-autoland system.

Airplane stability is affected by the wind shear: aerodynamic forces and moments are dependent on the components of wind speed, motion is dependent on aerodynamic forces and moments, and the components of wind speed are dependent on airplane motion. If the aerodynamic characteristics can be considered to be concentrated at the center of gravity, only longitudinal stability, principally phugoid or long period stability, is affected by wind shears.

A headwind shear can either stabilize or destabilize the phugoid, depending on the characteristics of the airplane's stability derivatives. If a headwind shear has stabilizing effects, a tailwind has destabilizing effects, and vice versa.

The effects of a wind shear may not be adequately represented by considering the aerodynamic characteristics to be concentrated at the center of gravity. Due to the change of wind speed with altitude, there is a distribution of wind speed over the vertical tail that introduces a rolling moment. When the airplane is disturbed from zero pitch attitude and wings level, the different parts of the airplane in the plane of the wings will be at different altitudes and there will be a distribution of wind speed about the airplane and a corresponding change in the distribution of lift.

The distribution of wind about the airplane may well be represented as being linear in three dimensions. Then the components of wind at some point (x,y,z) are represented by

$$\bar{u}_W = \bar{u}_{W_{CG}} + \frac{\partial \bar{u}_W}{\partial x} x + \frac{\partial \bar{u}_W}{\partial y} y + \frac{\partial \bar{u}_W}{\partial z} z$$

$$\bar{v}_W = \bar{v}_{W_{CG}} + \frac{\partial \bar{v}_W}{\partial x} x + \frac{\partial \bar{v}_W}{\partial y} y + \frac{\partial \bar{v}_W}{\partial z} z$$

$$\bar{w}_W = \bar{w}_{W_{CG}} + \frac{\partial \bar{w}_W}{\partial x} x + \frac{\partial \bar{w}_W}{\partial y} y + \frac{\partial \bar{w}_W}{\partial z} z$$

The derivative of body axis wind components are expressible in terms of the mean wind shear and can be interpreted as effective angular components of wind. For example, the distribution of the lateral component of wind

about the vertical dimensions of the fin appears as a roll rate, which generates a rolling moment proportional to the fin's contribution to the roll rate derivative of rolling moment.

Linear analysis predicts that the distributed lift effects of the mean wind shear appear primarily for lateral-directional motion. These effects are due to the headwind-tailwind component of the shear. The wind shear alters all of the lateral-directional stability characteristics, but the sensitivity of the characteristic roots to wind shear are configuration dependent.

Representation of the distributed lift effects is the only reason for computing the mean wind shear at each altitude. If the distributed lift effects can be shown to be insignificant, the computation of the shear can be left out of the simulation.

TURBULENCE

Analytic Description

For unstable atmospheric conditions, amplified displacement of air particles from their initial positions due to buoyancy forces cannot increase without bound. Turbulence is the mechanism by which the effects of instability are constrained through the mixing of hot and cold air particles, which produces equilibrium locally. The appearance and disappearance of turbulence with changing atmospheric stability involves a hysteresis effect, but it is predicted to occur at the critical Richardson's number, related to the log-linear mean wind profile constant:

$$R_{iCRIT} = \frac{1}{a'} = 0.222 \text{ for } a' = 4.5$$

The equations of motion for turbulence have been developed from the Navier-Stokes equations, but the severe nonlinearity of these equations has prevented their solution. Even if they could be solved, it is questionable as to whether they could be practically applied. From observations relating to these equations, some characteristics have been determined:

- Turbulence transports energy from large eddies, where it is generated mechanically and thermally to smaller eddies until it is finally dissipated viscously.
- Turbulence can only occur nonlinearly in three dimensions.
- Turbulence is diffusive and far more efficient for the transport of mass, momentum, and heat properties than molecular motion.
- Turbulence is a continuum having a smallest dynamically significant scale much larger than molecular or intermolecular dimensions.
- Turbulence is approximately an equilibrium phenomenon for homogeneous terrain having very low rates of change of kinetic energy.
- The diffusive, continuous, and equilibrium characteristics tend to produce homogeneity for turbulence in a horizontal plane,

Using these properties of turbulence, a statistical description of turbulence is developed. The basic statistical function is the average product of two turbulence components measured at two points of time and space, the correlation function:

$$R_{ij}(t_1,t_2,\vec{r_1},\vec{r_2}) = \overline{u_i(t_1,\vec{r_1})u_j(t_2,\vec{r_2})}$$

When $\vec{r_1} = \vec{r_2}$ (measured at the same point in space) and $t_1 = t_2$ (measured at the same time), the correlation function becomes the covariance. When, in addition, i = j, the correlation function is the variance.

By invoking homogeneity (turbulence properties independent of absolute position in space) and stationarity (turbulence properties independent of absolute time), the parameters reduce to just the displacements in position and time between the measured components:

$$R_{ij}(t_1, t_2, r_1, r_2) = R(\tau\ \vec{\xi})$$

$$\tau = t_2 - t_1$$

$$\xi = \vec{r_1} - \vec{r_2}$$

By additionally applying Taylor's hypothesis (frozen field concept), which assumes airplanes fly at speeds large compared to turbulent velocities and their rates of change, the time displacement can be related to a component of the position displacement, leaving statistical turbulence properties defined only in terms of space.

The correlation function can be transformed into the three-dimensional spectrum function by applying the Fourier integral:

$$\theta_{ij}(\vec{\Omega}) = \frac{1}{(2\pi)^3} \int_{-\infty}^{\infty} R_{ij}(\vec{\xi}) e^{-i\vec{\Omega}\vec{\xi}}\, d\vec{\xi}$$

The parameter $\vec{\Omega}$ is the spacial frequency vector having units of rad/ft and is related to distance as temporal frequency in rad/sec is to time. The transformation can be reversed by the inversion formula:

$$R_{ij}(\vec{\xi}) = \int_{-\infty}^{\infty} \theta_{ij}(\vec{\Omega}) e^{i\vec{\Omega}\vec{\xi}} d\vec{\Omega}$$

When $\vec{E} = 0$, the correlation function becomes the covariance and the spectrum function can be seen to be the distribution of the covariance with spacial frequency:

$$\sigma_{ij}^2 = \int_{-\infty}^{\infty} \theta_{ij}(\vec{\Omega}) d\vec{\Omega}$$

Simulation of turbulence can be performed only by a temporal process, but only one component of spacial frequency (that in the direction of flight) can be related to time or temporal frequency through Taylor's hypothesis, $\omega = \Omega_1 V_A$. To obtain a spectrum function in terms of the component associated with the coordinate in the direction of flight ($\Phi(\Omega_1)$) integration of the spectrum function over the other two Components is performed. Then

$$\sigma_{ij}^2 = \int_{-\infty}^{\infty} \Phi(\Omega_1) d\Omega_1$$

Important characteristics of the one-dimensional spectrum function, $\Phi_{ij}(\Omega_1)$, have been derived by Batchelor for the special case of isotropic turbulence, for which the statistical properties of turbulence are invariant with coordinate system rotation or translation. Batch'elor showed that there were but two one-dimensional spectrum functions: one for two parallel longitudinal turbulence components (components aligned to the vector separating them), $\Phi_{PP}(\Omega_1)$, and one for parallel transverse components (components

normal to the vector separating them), $\Phi_{NN}(\Omega_1)$. All spectra for orthogonal components are zero. The variances for all components are equal. The two spectra are related by

$$\Phi_{NN}(\Omega_1) = \frac{1}{2}\left[\Phi_{PP}(\Omega_1) - \Omega_1 \frac{d\Phi_{PP}(\Omega_1)}{d\Omega_1}\right]$$

Determination of one of the isotropic spectrum functions provides the other.

Corresponding to the two spectrum functions are two nondimensional (divided by variance) scalar correlation functions: one, $f(\xi)$, for two parallel longitudinal components, and the other, $g(\xi)$, for two parallel transverse components, which are also interrelated:

$$f(\xi) = \frac{\overline{u_P^2}(\xi)}{\sigma_2}$$

$$g(\xi) = \frac{\overline{u_N^2}(\xi)}{\sigma_2}$$

$$g(\xi) = f(\xi) + \frac{\xi}{2}\frac{df(\xi)}{d\xi}$$

The fundamental correlation functions are analogous to serial correlation functions.

A measure of the average eddy size, the integral scale may be determined from the fundamental correlation functions:

$$L_P = \int_0^\infty f(\xi)\,d\xi$$

$$L_N = \int_0^m g(\xi)\,d\xi$$

For a separation distance, ξ, equal to the integral scale, the area under the corresponding correlation function is divided into equal parts. Through the relationship between the fundamental correlation functions, it can be shown

$$L_P = 2 L_N$$

The integral scales provide means for normalizing distance. It is then postulated that $f(\xi/L_P)$ and $g(\xi/L_N)$ are universal functions. The one-dimensional spectrum functions must correspondingly have the form

$$\Phi_{ii}(\Omega_1) = \sigma ii^2 G(L_i, L_i \Omega_1) .$$

That is, spacial frequency appears only in combination with the integral scales.

Theory and empirical investigation have led to additional requirements for the isotropic one-dimensional spectra:

- The high frequency asymptotes (excluding viscous dissipation) of the spectra are of the form $\Phi_{ii}(\Omega_1) \sim \Omega^{-5/3}$ This leads to a ratio of the transverse-to-longitudinal spectrum equal to *4/3* at high frequencies.
- The low-frequency asymptotes are frequency invariant. This leads to a ratio of the transverse-to-longitudinal spectrum equal to 1/2.
- Isotropic spectra must be symmetric about $\Omega_1 = 0$.

A number of isotropic spectra forms have been proposed. The best-known forms for aeronautical applications are the Dryden and von Karman forms, presented with related functions in Figure 18.

Van Karman	Dryden

Longitudinal correlation function:

$$f(\xi) = \frac{2^{2/3}}{\Gamma(1/3)}\left(\frac{\xi}{aL}\right)^{1/3} K_{1/3}\left(\frac{\xi}{aL}\right) \qquad f(\xi) = e^{-\xi/L}$$

Transverse correlation functions:

$$g(\xi) = \frac{2^{2/3}}{\Gamma(1/3)}\left(\frac{\xi}{aL}\right)^{1/3}\left[K_{1/3}\left(\frac{\xi}{aL}\right) - \frac{\xi}{2aL} K_{2/3}\left(\frac{\xi}{aL}\right)\right] \qquad g(\xi) = e^{-\xi/L}\left[1 - \frac{\xi}{2L}\right]$$

Longitudinal one dimensional power spectrum:

$$\Phi_{pp} = \frac{\sigma^2 L}{\pi} \frac{1}{\left[1 + (aL\Omega_1)^2\right]^{5/6}} \qquad \Phi_{pp} = \frac{\sigma^2 L}{\pi} \frac{1}{\left[1 + (L\Omega_1)^2\right]}$$

Transverse one dimensional power spectrum:

$$\Phi_{NN} = \frac{\sigma^2 L}{2\pi} \frac{1 + 8/3\,(aL\Omega_1)^2}{\left[1 + (aL\Omega_1)^2\right]^{11/6}} \qquad \Phi_{NN} = \frac{\sigma^2 L}{2\pi} \frac{1 + 3(L\Omega_1)^2}{\left[1 + (L\Omega)^2\right]^2}$$

Energy spectrum:

$$E(\Omega) = \frac{55}{9\pi}\sigma^2 L \frac{(aL\Omega)^4}{\left[1 + (aL\Omega)^2\right]^{17/6}} \qquad E(\Omega) = \frac{8\sigma^2 L}{\pi} \frac{(L\Omega)^4}{\left[1 + (L\Omega)^2\right]^3}$$

Definitions:

$a = 1.339$

$\Omega = |\vec{\Omega}| = |\Omega_1 \hat{i} + \Omega_2 \hat{j} + \Omega_3 \hat{k}|$

Φ_{pp} and Φ_{NN} such that $\sigma^2 = \int_{-\infty}^{\infty} \Phi_{pp}\, d\Omega_1 = \int_{-\infty}^{\infty} \Phi_{NN}\, d\Omega_1$

$$L = \int_0^{\infty} f(\xi)\, d\xi = 2\int_0^{\infty} g(\xi)\, d\xi$$

$K_{1/3}\left(\frac{\xi}{aL}\right)$ and $K_{2/3}\left(\frac{\xi}{aL}\right)$ are modified Bessel functions of the second kind.

FIGURE 18 – VON KARMAN AND DRYDEN CORRELATION AND SPECTRA FUNCTIONS

The Dryden form is simpler and is based on an exponential shape of the fundamental correlation functions. The Dryden function fails to meet the high-frequency requirement.

The von Karman forms result from a curve fitting expression for the energy spectrum and satisfy all isotropic requirements. In numerous investigations the von Karman forms have been shown to be superior to the Dryden forms. The von Karman one-dimensional spectra are those accepted for the model.

Although high-altitude turbulence is well represented by isotropy, low-altitude turbulence is clearly nonisotropic. Specifically:

- The statistical functions describing the field of turbulence are not invariant with coordinate rotation; variances of turbulence components are not equal and the longitudinal and transverse integral scales vary with coordinate rotations.
- Low-altitude turbulence exhibits a lack of homogeneity with altitude; the variances and integral scales of turbulence vary with altitude.
- A non-zero correlation between turbulence in the direction of the mean wind and vertical turbulence has been found. Isotropic turbulence requires zero correlation between orthogonal components.

There are, however, limited conditions of isotropy found to hold for low-altitude turbulence:

- At sufficiently high spacial frequencies (short separation distances), low-altitude turbulence is isotropic. This is referred to as "local isotropy" and requires the high-frequency spectrum asymptotes to be invariant with coordinate rotations.

- The existence of a single non-zero correlation function between the downwind and vertical components of turbulence is compatible with horizontal isotropy (invariance of the horizontal statistical functions with rotations of the axis system in the horizontal plane). Horizontal isotropy must be viewed as an approximate characteristic for low-altitude turbulence, for the variance of horizontal turbulence perpendicular to the mean wind is frequently reported as being somewhat greater than the variance of the component in the direction of the mean wind.

The spectra that have been developed specifically for low altitude tend to be for small regions of altitude near the surface and do not tend to full isotropy at higher altitudes. A frequently employed technique that is employed in this report is to adopt isotropic spectra for low altitude by permitting the variances and integral scales to be different for each component. The von Karman spectra are used. These low-altitude forms become:

$$\Phi_u(\Omega_1) = \frac{\sigma_u^2 L_u}{\left[1+(1.339\ L_u\Omega_1)^2\right]^{5/6}}$$

$$\Phi_v(\Omega_1) = \frac{\sigma_v^2 L_v}{2\pi}\ \frac{1+8/3(1.339\ L_v\Omega_1)^2}{\left[1+(1.339\ L_v\Omega_1)^2\right]^{11/6}}$$

$$\Phi_w(\Omega_1) = \frac{\sigma_w^2 L_w}{2\pi}\ \frac{1+8/3(1.339\ L_w\Omega_1)^2}{\left[1+(1.339\ L_w\Omega_1)^2\right]^{11/16}}$$

These spectra were originally written in terms of the longitudinal integral scale, which is twice the transverse integral scale for isotropy, so L_v and L_w must be redefined as twice the area under the corresponding correlation functions,

Although a cross spectrum, Φ_{uw}, has been found to exist, it has been concluded that the cross spectrum has a significant magnitude only at frequencies too low to be important.

Simulator Representation of Turbulence Spectra

The spectra in terms of temporal frequency are obtained by substituting $\Omega_1 = \omega/V_A$ (Taylor's hypothesis) and by requiring the variance to be the same in either domain:

$$\sigma_i^2 = \int_{-\infty}^{\infty} \Phi_i(\omega)\, d\omega = \int_{-\infty}^{\infty} \Phi_i(\Omega_1)\, d\Omega_1$$

Then

$$\Phi_i(\omega) = \frac{1}{V_A} \Phi_i \left(\Omega_1 = \frac{\omega}{V_A} \right)$$

When a random variable is modified by a transfer function, the output spectrum is given by

$$\Phi_O(\omega) = M^2(\omega)\, \Phi_N(\omega)$$

where:

$\Phi_O(\omega)$ = output spectrum

$M(\omega)$ = amplitude frequency response of the transfer function

$\Phi_N(\omega)$ = power spectrum of the random function or noise

Turbulence is represented by finding a transfer function such that

$$M(\omega) = \sqrt{\frac{\Phi_O(\omega)}{\Phi_N(\omega)}}$$

where the output frequency response is equal to that desired. When white noise is used, $\Phi_N = 1$ by definition. Then to match a desired power spectrum, it is only necessary to find a transfer function with a frequency response equal to the square root of the spectrum.

It is not possible to exactly reproduce the von Karman spectra with linear transfer functions (filters) due to exponents of frequency that are noneven integers, so an approximation is sought.

The significant criteria for evaluating an approximation to a power spectra is to require the contribution of each incremental frequency range to the variance to be correct for the frequency range in which the airplane's response is important. Directly plotting $\Phi(\omega)$ versus ω lacks resolution over the entire frequency range. Plots of $\omega\Phi(\omega)$ versus log (w) provide the necessary resolution and the area under such a curve is also equal to the contribution to the variance:

$$\Delta\sigma^2 = \int_{\omega_1}^{\omega_2} \Phi(\omega)\,d\omega = \int_{\text{Log } \omega_1}^{\text{Log } \omega_2} \omega\Phi(\omega)\,d(\log \omega)$$

The validity of transfer functions representing spectra may be assessed by comparing plots of this type for the transfer function frequency response squared and the power spectrum.

Filters exactly duplicating the Dryden spectra are often assumed to match the von Karman spectra well for rigid airplane responses even though it is conceded the Dryden spectra are not substantiated by theory and empirical evidence. This is seen not to be true in Figure 19, for the Dryden spectra provide greater contributions to the variance than the von Karman spectra by as much as 25% at frequencies where contributions to the variance are greatest. Approximate filters that do a much better job of matching the von Karman spectra are presented in Figure 20 (where the corresponding mechanization is also shown). Comparisons of the filters in Figure 20 with the von Karman spectra are shown in Figures 21 and 22.

The white noise may be generated by either hardware or software (digitally), There are several methods available, each with different shortcomings.

When the noise is generated digitally, it is only approximately random and the noise spectrum is only approximately flat and equal to one. The digital generation of white noise consists of three main steps:

1) Random numbers having a uniform distribution between 0 and 1 are generated.
2) From the uniform distribution, the distribution assumed to hold for turbulence is generated.
3) The noise thus far produced will have a unit variance and a spectrum amplitude of $\Delta t/2\pi$ (At = frame time or sampling interval) no matter what distribution is used in 2). To provide white noise for which the spectrum amplitude is one, the output from 2) is multiplied by $\sqrt{2\pi/\Delta t}$.

Turbulence velocities within a single patch of turbulence are assumed to form a Gaussian distribution. Although

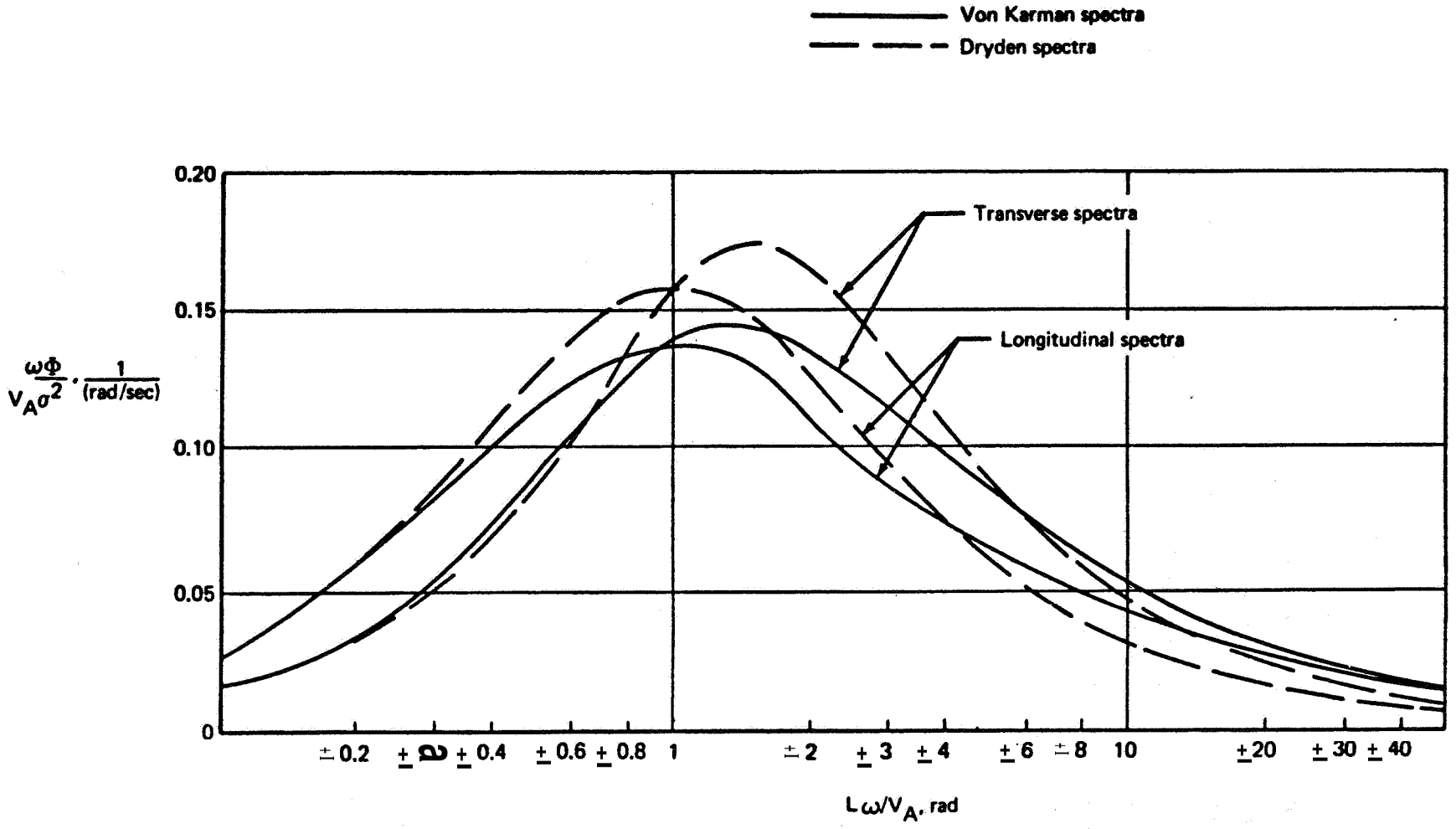

FIGURE 19 – COMPARISON: DRYDEN AND VON KARMAN VARIANCE DENSITY

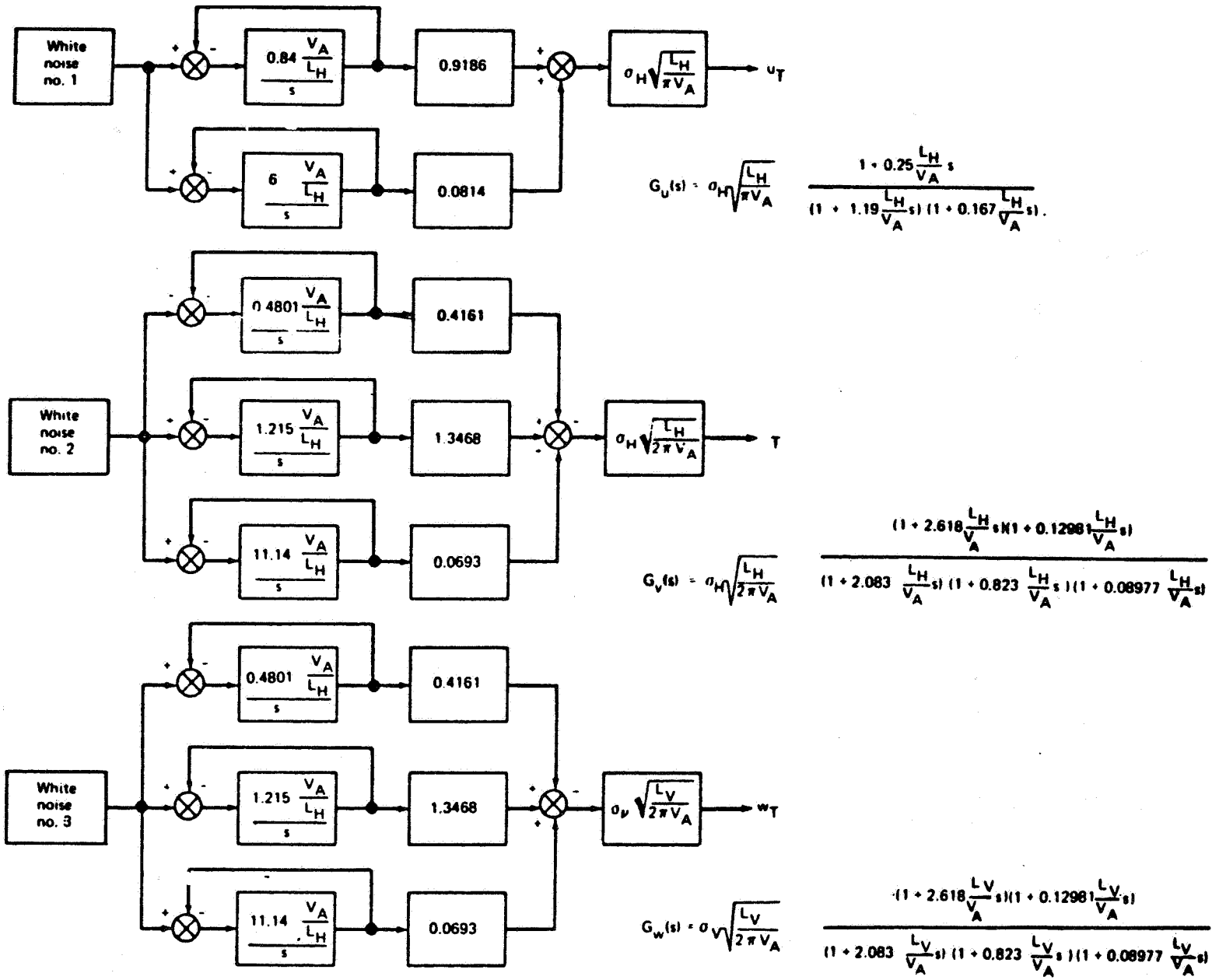

FIGURE 20 – SCHEMATIC FOR TURBULENCE FILTERS

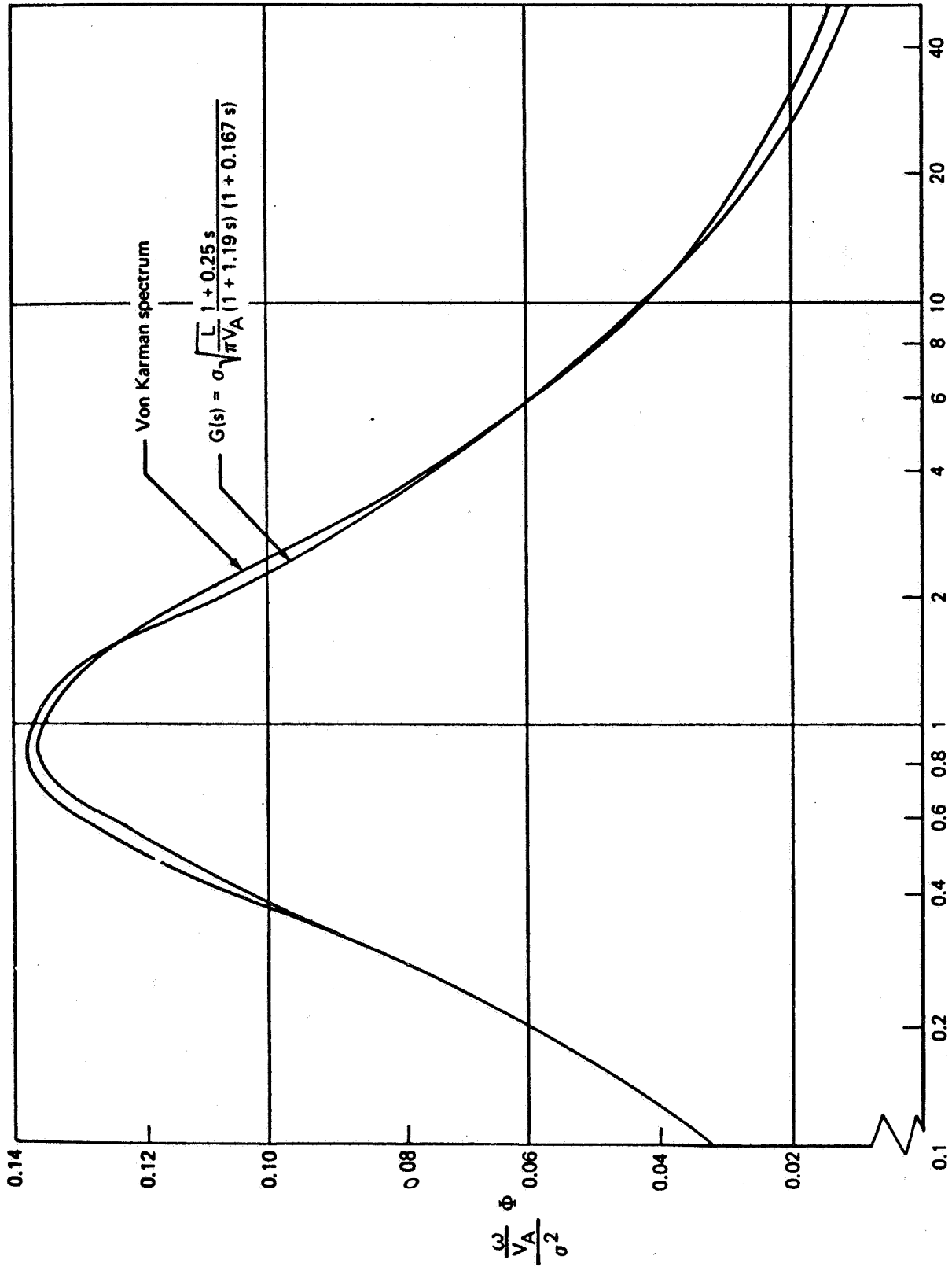

FIGURE 21 – APPROXIMATE LONGITUDINAL TURBULENCE FILTER ACCURACY

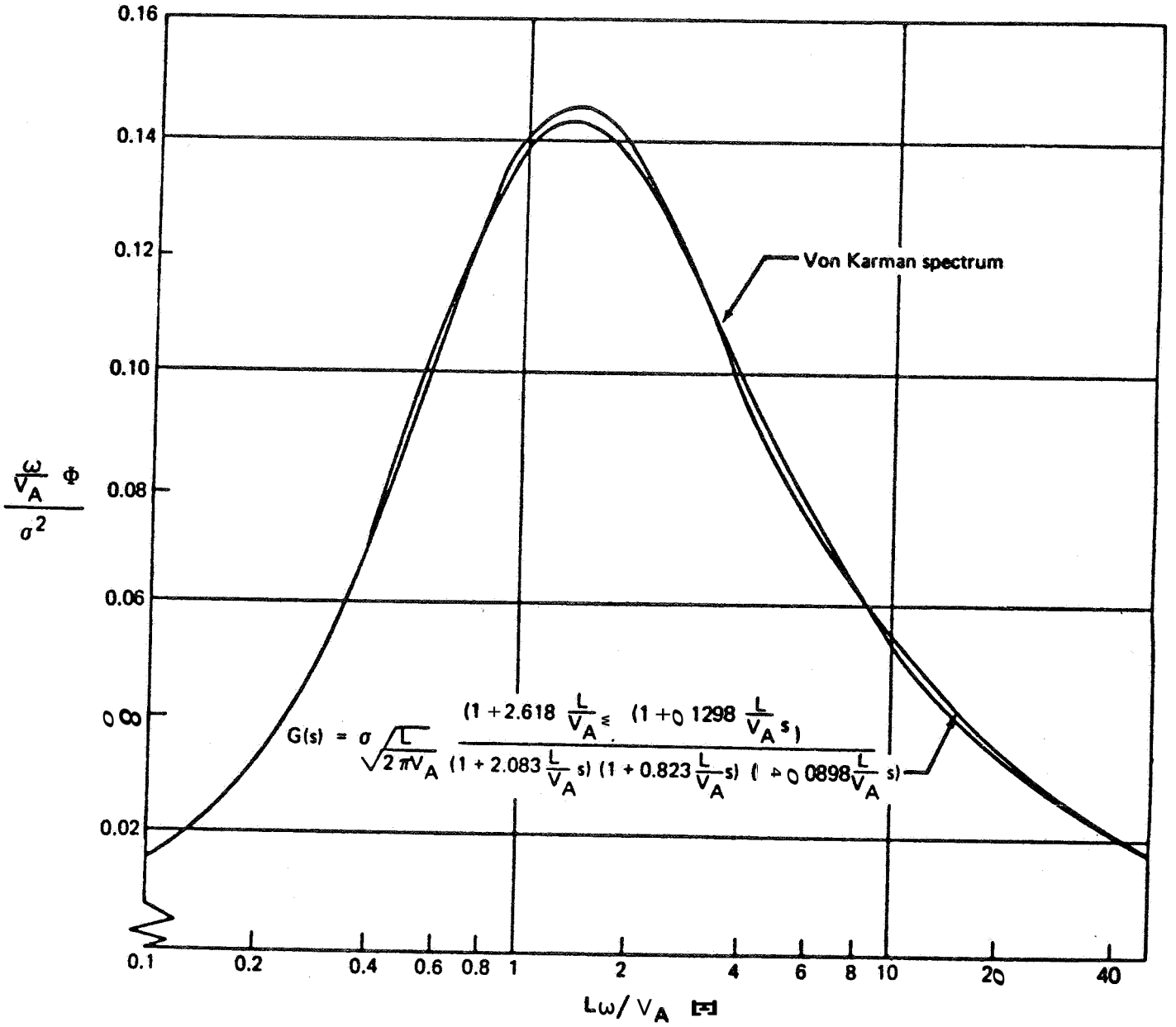

FIGURE 22 – APPROXIMATE TRANSVERSE TURBULENCE FILTER ACCURACY

the distribution of turbulence velocities for the sum of all turbulence patches have been shown to be non-Gaussian, this is not inconsistent with a Gaussian distribution for a single patch of turbulence.

Turbulence Scale and Magnitude

The simulator model for turbulence in Figure 20 lacks definition of the variances and integral scales. The measurements and theory for these statistical parameters of turbulence are measured in an axis system aligned to the mean wind.

Dimensional analysis leads to a description of the vertical turbulence standard deviation for unstable conditions

$$\frac{\sigma_w}{u_*} = C\left[\frac{kh}{u_*}\frac{\partial \bar{V}_W}{\partial h} - \left(\frac{D}{C}\right)^3 \frac{h}{\ell'}\right]^{1/3}$$

D and C are constants

For neutral conditions where the nondimensional shear at the surface $(kh/u_*)/\partial \bar{V}_W/\partial h)$, is 1,

$$\frac{\sigma_w}{u_*} = 1.3 = C$$

is well accepted. For extremely unstable conditions, the nondimensional shear is negligible and the equation reduces to

$$\frac{\sigma_w}{u_*} = D\left(-\frac{h}{\ell'}\right)^{1/3}$$

The constant, D, is well represented by 1.7, hence

$$\frac{\sigma_w}{u_*} = 1.3\left[\left(\frac{kh}{u_*}\frac{\partial \bar{V}_w}{\partial h}\right) - 2.236\left(\frac{h}{\ell'}\right)\right]^{1/3}$$

The nondimensional shear has been described as a function of h/ℓ' only, so σ_w/u_* is also completely described by h/ℓ'. For near neutral conditions and slightly stable conditions, the shape of σ_w/u_* versus h/ℓ' has been made to match that of measured data. The standard deviation of vertical turbulence is reduced abruptly beginning at $h/\ell' = 1$, above which the nondimensional shear is constant, to $\sigma_w/u_* = 0$ at $h/\ell' = 1.22$, which corresponds to the critical Richardson's number ($Ri_{CRIT} = 0.222$). The combined description for σ_w/u_* is presented in Figure 23. The procedure for computing the ms level of turbulence vertical to the earth is:

$$\sigma_w = u_*\left[\frac{\sigma_w}{u_*}\left(\frac{h}{\ell'}\right)\right]$$

$$= 0.4\bar{V}_{20}\left(\frac{u_{*_0}/k}{\bar{V}_{20}}\right)\left(\frac{u_*}{u_{*_0}}\right)\left[\frac{\sigma_w}{u_*}\left(\frac{h}{\ell'}\right)\right]$$

where:

$\frac{u_{*_0}/k}{\bar{V}_{20}}$ determined for the mean wind model

$\frac{u_*}{u_{*_0}} = 1 - \frac{h}{d}$, as determined from the mean wind model

$d = 2000\, u_{*_0}$, as determined for the mean wind model

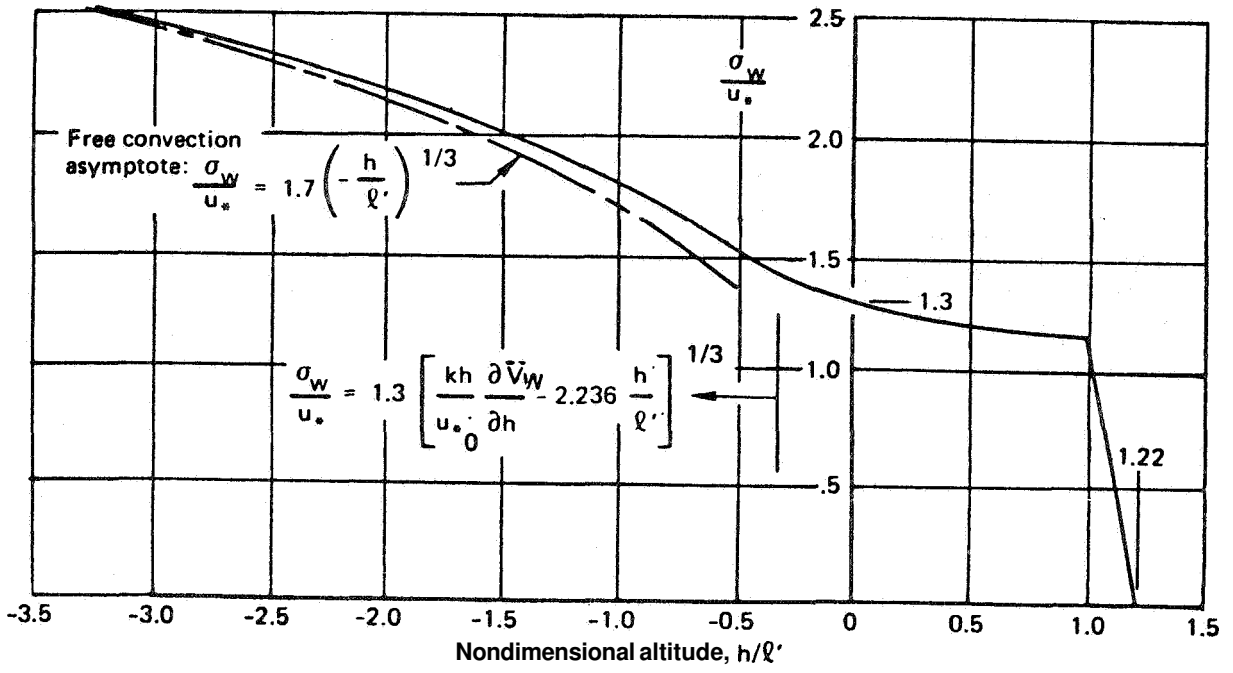

FIGURE 23 – σ_W/u_* VARIATION WITH STABILITY

The standard deviation for vertical turbulence is described as being proportional to the mean wind speed at 20 feet, as decreasing and finally disappearing with increasing atmospheric stability, and as tending toward zero as altitude approaches the boundary layer. The variation of σ_W with altitude for different surface wind and atmospheric stability conditions is shown in Figure *24.*

Dimensional analysis relationships for the variances of horizontal components of turbulence have not had good empirical support. At the surface, the magnitudes of the horizontal components are significantly greater than magnitude of the vertical component with the component in the direction of the mean wind frequently reported as greater than the horizontal component normal to the mean wind. The

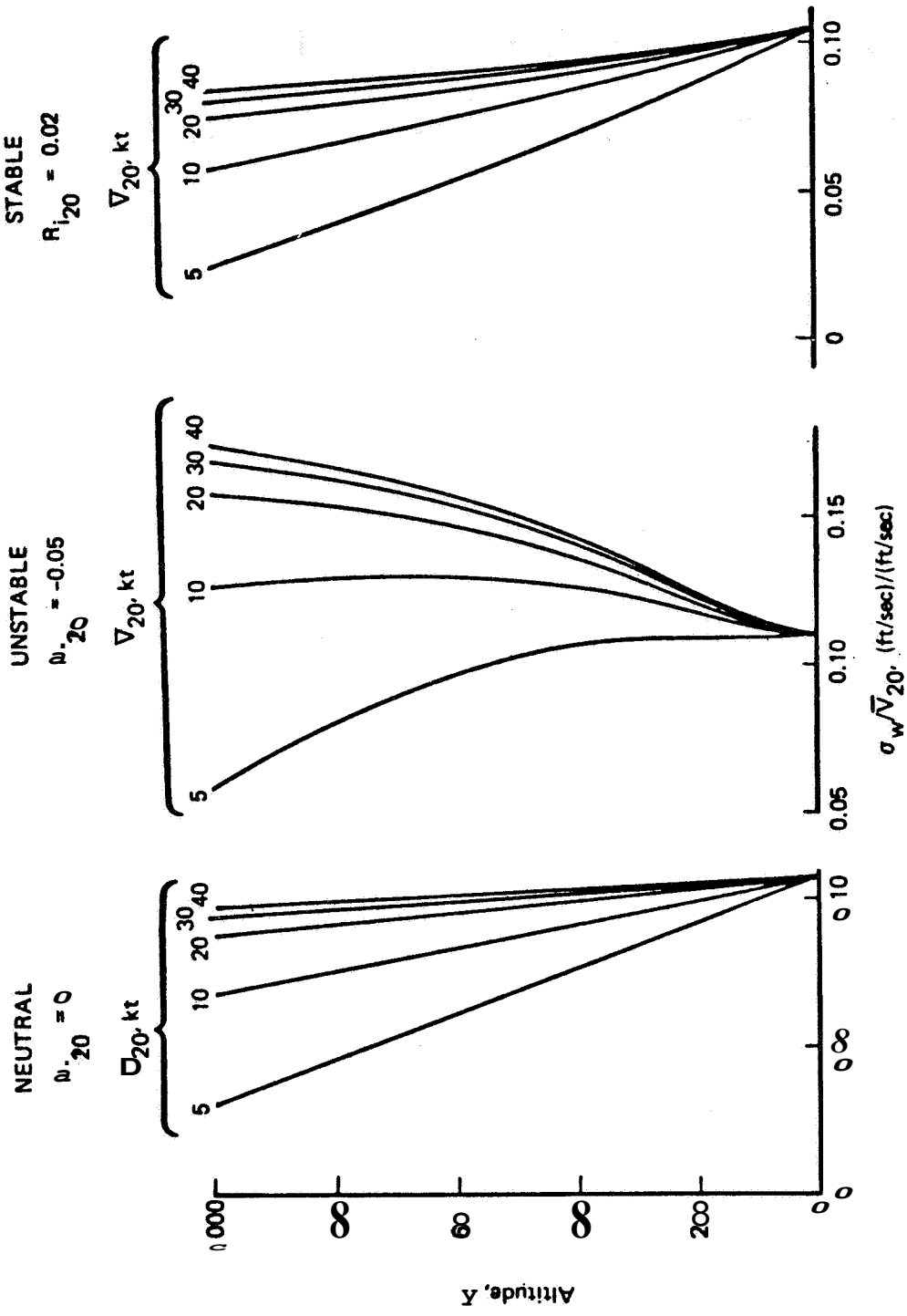

FIGURE 24 – PROFILE OF VERTICAL TURBULENCE RMS, SELECTED DESCRIPTION

data do not indicate any clear relationship between the variances for the horizontal turbulence components but do show them to be approximately equal, so horizontal isotropy ($\sigma_u = \sigma_v$, $L_u = L_v$) is assumed. This enables describing turbulence characteristics according to whether turbulence components are vertical or horizontal. A corresponding change of nomenclature is adopted: σ_V replaces σ_w, L_V replaces L_w, σ_H replaces σ_u and σ_v, and L_H replaces L_u and L_v (subscripts **H** and V refer to horizontal and vertical components).

The change in nomenclature aids in differentiating between turbulence components aligned to the mean wind and turbulence components aligned to other axis systems.

It is assumed that the horizontal components of turbulence have variances that change identically with stability. Qualitatively, this is not correct, but any other quantitative descriptions based on the information in hand would be just as arbitrary but more complex. As a result, the standard deviation for horizontal turbulence may be described by

$$\sigma_H = \left(\frac{\sigma_H}{\sigma_V} \right) \sigma$$

At the surface $\sigma_H/\sigma_V = 2$ is a good compromise of the data. Above a sufficiently high altitude where complete isotropy begins, h_I, $\sigma_H/\sigma_V = 1$. There is little information to describe the variation of σ_H/σ_V with altitude, so an interpolation equation,

$$\frac{\sigma_H}{\sigma_V} = \begin{cases} \dfrac{1}{\left[0.177 + 0.823 \dfrac{h}{h_I} \right]^{0.4}}, & h < h_I \quad \text{(Fig. 25)} \\ 1, & h \geq h_I \end{cases}$$

$$\frac{\sigma_u}{\sigma_w} = \frac{\sigma_v}{\sigma_w} = \begin{cases} \left[0.177 + 0.823\, h/h_l\right]^{.4} & , h < h_l \\ 1.0 & , h \geq h_l \end{cases}$$

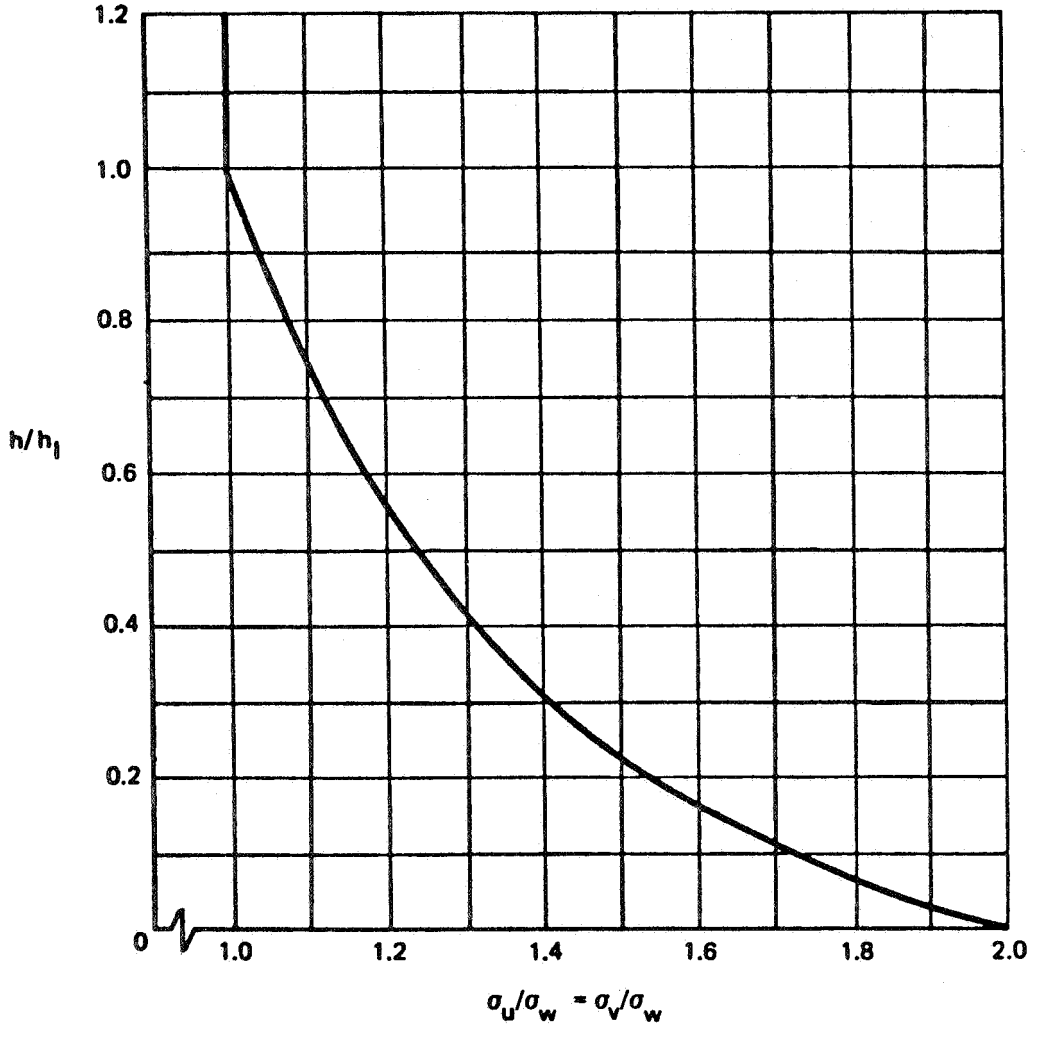

FIGURE 25 – SELECTED DESCRIPTION FOR VARIANCES OF HORIZONTAL TURBULENCE COMPONENTS

was developed that is qualitatively similar to other variations proposed.

Implied estimates for the altitude above which isotropy exists (h_I) range from 300 to 2500 feet. The latter number is an extreme. A value of h_I = 1000 feet is chosen, is adequately supportable, and provides integral scales comparable with other models.

The integral scale for vertical turbulence is predicted by dimensional analysis to have the form

$$L_V = [B(R_i)]h$$

That is, the vertical turbulence integral scale is linearly related to altitude with the proportionality constant dependent upon stability.

The atmospheric stability dependence of the proportionality constant is apparently weak, at least for a wide range of stability conditions, and is assumed to be constant. Estimates for B range from 0.125 to greater than *4*, with most estimates centered about 0.5 and 1. Unit proportionality is assumed. The estimates about 0.5 may be for the literal definition of integral scale equal to the integral of the correlation function rather than the redefinition of twice that area. Hence, the estimates of 0.5 may be consistent with the unit proportionality assumed for the redefinition. In keeping with isotropy about 1000 feet, L_V = 1000 feet for h $\geq$ 1000 feet.

The integral scale for horizontal turbulence is the parameter for which knowledge is poorest. It may be derived from the condition of local isotropy at low altitudes, which can be shown to require:

$$L_H = \left(\frac{H}{V}\right)^3 L_V \qquad \text{(Fig. 26)}$$

$$L_w = \begin{cases} h, h < h_1 \\ d, h = h_1 \end{cases}$$

$$L_u = \begin{cases} L_w \left(\frac{\sigma_u}{\sigma_w}\right)^3 = \frac{h}{\left[0.177 + 0.823\, h/h_1\right]^{1.2}} & , h < h_1 \\ d & , h \geq h_1 \end{cases}$$

$$L_v = L_u$$

h_1 = Altitude above which turbulence is isotropic

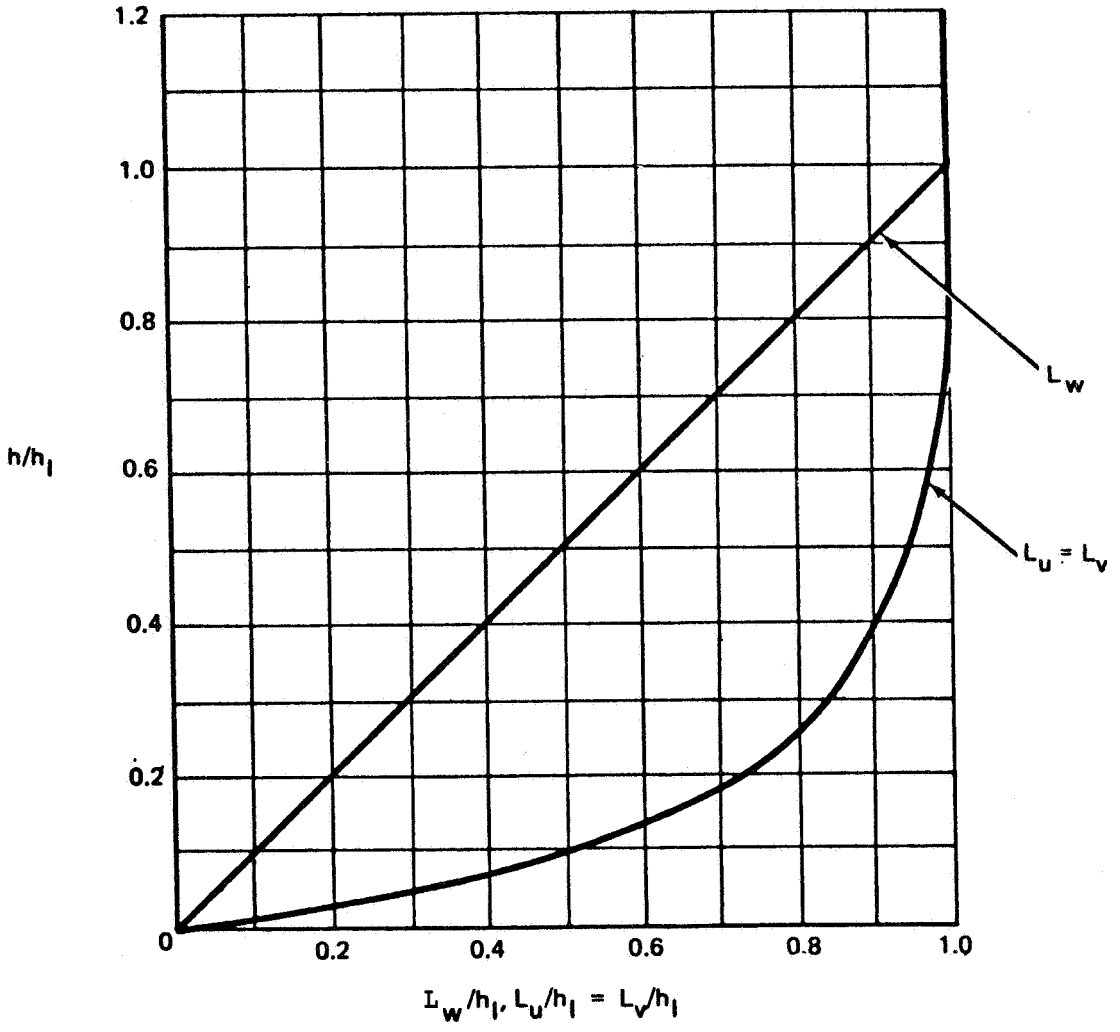

FIGURE 26 – SELECTED INTEGRAL SCALE DESCRIPTION

This description provides a horizontal turbulence integral scale greater or equal to that vertical turbulence. At the surface, $L_H = 8\ L_V$. Above 1000 feet, where isotropy is assumed to exist, the integral scales are equal. These characteristics are in agreement with observations.

Turbulence Axis Systems

There is an inconsistency in the turbulence model developed: the power spectra are for turbulence components aligned to the airplane's velocity with respect to the air mass and the standard deviations and integral scales are for turbulence components aligned with respect to the plane of the earth and the mean wind heading. Both sets of components can, in general, coincide only for an observer whose position with respect to the earth is fixed.

One exact approach for resolving the differences in axis systems consists of transforming the variances and integral scales from the mean wind axis system to the axis system attached to the relative wind where the spectra shapes are known. Turbulence components would then be generated in the relative wind axis and transformed to the body axis. Transformations for the integral scales and variances have been developed, but are quite complex. Complete tensor transformations have been developed and reveal that when the airplane's relative velocity is not aligned to the mean wind and when wings are nonlevel, nonnegligible cospectra exist in the body axis (components of body axis turbulence are correlated). Since the power spectra shapes are in general not known in the mean wind axis system and the cospectra forms are not known for a body axis system, the exact method cannot be performed.

Errors from approximate methods were examined. It was revealed that for low-altitude turbulence, it is much more

important to have the correct alignment for the variances and integral scales than for the spectra shapes. The greatest error in the spectra magnitude at any frequency for turbulence normal to the airplane that can occur due to misalignment of the spectra shape is a factor of 2, while the greatest error possible due to misalignment of the statistical parameters is a factor of 64. The best compromise found was to generate turbulence in an axis system that is in the plane of the earth but aligned to the heading of the airplane's relative velocity vector with the filters in Figure 20 and the specified rms levels and integral scales. The components of turbulence are then transformed to the body axis system. The transformation required is presented in Figure 16.

Application to Aerodynamics

When the aircraft can be adequately represented as though the aerodynamic forces and moments were concentrated at the center of gravity, turbulence affects forces and moments through the computation of body axis velocities relative to the air mass:

$u_A = u - u_W, u_W = \bar{u}_W + u_T$

$v_A = v - v_W, v_W = \bar{v}_W + v_T$

$w_A = w - w_W, w_W = \bar{w}_W + w_T$

$V_A = u_A^2 + v_A^2 + w_A^2$

u,v,w = inertial velocity components along the x, y, and z body axis coordinates

$u_A\ v_A\ w_A$ = components of airplane velocity relative to the air mass

$u_W\ v_W\ w_W$ = components of wind relative to the earth

$\bar{u}_W\ \bar{v}_W\ \bar{w}_W$ = components of mean wind relative to the earth

$u_T\ v_T\ w_T$ = components of turbulence velocities relative relative to the earth

The relative velocity components are used to determine the parameters, which in turn determine the aerodynamics forces and moments:

$$a = \tan^{-1}\frac{w_A}{u_A} = \text{angle of attack}$$

$$\beta = \sin^{-1}\frac{v_A}{V_A} - \text{sideslip angle}$$

$$\bar{q} = \frac{1}{2}\rho V_A^2 = \text{dynamic pressure}$$

$$\dot{a} = \frac{u_A\dot{w} - w_A u}{u_A^2 + w_A^2}$$

$$\dot{\beta} = \frac{(u_A^2 + w_A^2)\dot{v} - v_A(\dot{u}_A u + w_A\dot{w})}{V_A^2\sqrt{u_A^2 + w_A^2}}$$

Note that for the point representation, $\dot{u}_W = \dot{v}_W = \dot{w}_W = 0$.

The attenuation of the high-frequency response of forces and moments due to the fact that lift cannot respond instantaneously to changes in angle of attack (unsteady aerodynamics) can be handled approximately through use of the Kussner and Wagner lift growth functions,

In general, it is not adequate to assume the aerodynamics may be represented by a point for the purpose of

simulating the effects of turbulence; there is a distribution of turbulence about the airplane that causes a change in the distribution of lift. The point representation has been estimated to be accurate only up to:

$\lambda_1 > 120\ell_T$

$\omega < 60\bar{c}$ for tailless aircraft or for the wing only

or

$< 0.1\ V_A/\ell_T$

$< 0.05\ \frac{V_A}{\bar{c}}$ for tailless aircraft or for the wing only

$\lambda_2 > \pi b$

where :

λ_1, λ_2 = wavelengths in the longitudinal and lateral directions, respectively

ℓ_T = tail length

b = wing span

$\bar{c}$ = mean chord

Only one method of representing all the distributed lift effects suitable for simulation has been found. This method represents the distribution of turbulence linearly, just as was done for the distributed lift effects of the mean wind. The derivatives of turbulence with respect to the coordinates are related to effective angular components of turbulence :

Effective Turbulence Angular Velocities

Wing	Tail
$p_T = -\frac{\partial w_T}{\partial y}$	$p_T = \frac{\partial v_T}{\partial z}$
$q_T = \frac{\partial w_T}{\partial x}$	$q_T = \frac{\partial w_T}{\partial x}$
$r_T = \frac{\partial u_T}{\partial y}$	$r_T = -\frac{\partial v_T}{\partial x}$

p_T, q_T, r_T = effective body axis roll, pitch, and yaw rates due to turbulence with respect to the earth

The effective angular velocities are generated through matching the spectra for the turbulence derivatives and their cospectra with the linear velocities of turbulence in a manner similar to that used for generating linear components of turbulence.

The effective angular velocities affect body axis forces and moments in the same way as did the linear components of turbulence. For example, the yaw rates of the airplane with respect to the air mass are computed by

$$r_A = r - r_W, \quad r_W = \bar{r}_W + r_T$$

Separate yaw rates for wing and tail are computed as the effective yaw rates of the wind are different. A total force or moment due to yaw rate is the sum of the contribution of the wing force or moment derivative with respect to yaw rate times the wing yaw rate with respect to the air mass and the contribution of the tail to the force or moment

derivative with respect to yaw rate times the tail yaw rate with respect to the air mass.

At lower and lower turbulence frequencies, the linear representation of the distribution becomes exact. The linear distribution becomes poor at high frequencies; relating effective angular velocities to turbulence derivatives produces infinite variances of angular velocities due to the error of the representation at high frequencies. The spectra for the angular velocities must be attenuated at high frequencies or truncated.

A comparison of representing the distribution of turbulence in this manner with the point representation has been made and it is concluded that a factor of 10 improvement in the maximum frequency to which the representation is valid occurs for representing the longitudinal distributions. This does not mean that the lateral and vertical distributions of turbulence are insignificant, just that they cannot be accurately modeled. However, from a simpler analysis, it is concluded that the rolling moment due to turbulence roll rate will generally be insignificant compared to the roll rate caused by the lateral component of turbulence.

The power spectra and cross spectra for turbulence pitch and yaw rates that provide longitudinal distributions of turbulence are represented by simply filtering the vertical and lateral components of turbulence by

$$q_T = -\frac{1}{V_A}\,\frac{s}{1+\frac{4\ell_T - s}{\pi V_A}}\,w_T$$

$$r_T = \frac{1}{V_A}\,\frac{s}{1+\frac{4\ell_T - s}{\pi V_A}}\,v_T$$

The terms $1/V_A$ s w_T and $1/V_A$ s v_T represent the derivatives of turbulence with respect to the longitudinal coordinate:

$$\frac{\partial}{\partial x} = \frac{\partial}{\partial t}\,\frac{dt}{dx} = \frac{1}{V_A}\,s$$

s = Laplace transform operator

The additional filter

$$\frac{1}{1+\frac{4\ell_T - s}{\pi V_A}}$$

attenuates the effective angular velocity at the maximum frequency to which the representation is valid assuming eight straight line segments are the minimum number that can adequately represent a sine wave. That is, the effective angular velocities are attenuated at a frequency corresponding to a wavelength that is eight times the distance over which the distribution of turbulence is provided. The power spectra that result are shown in Figure 27. There are also body axis accelerations due to distributed lift:

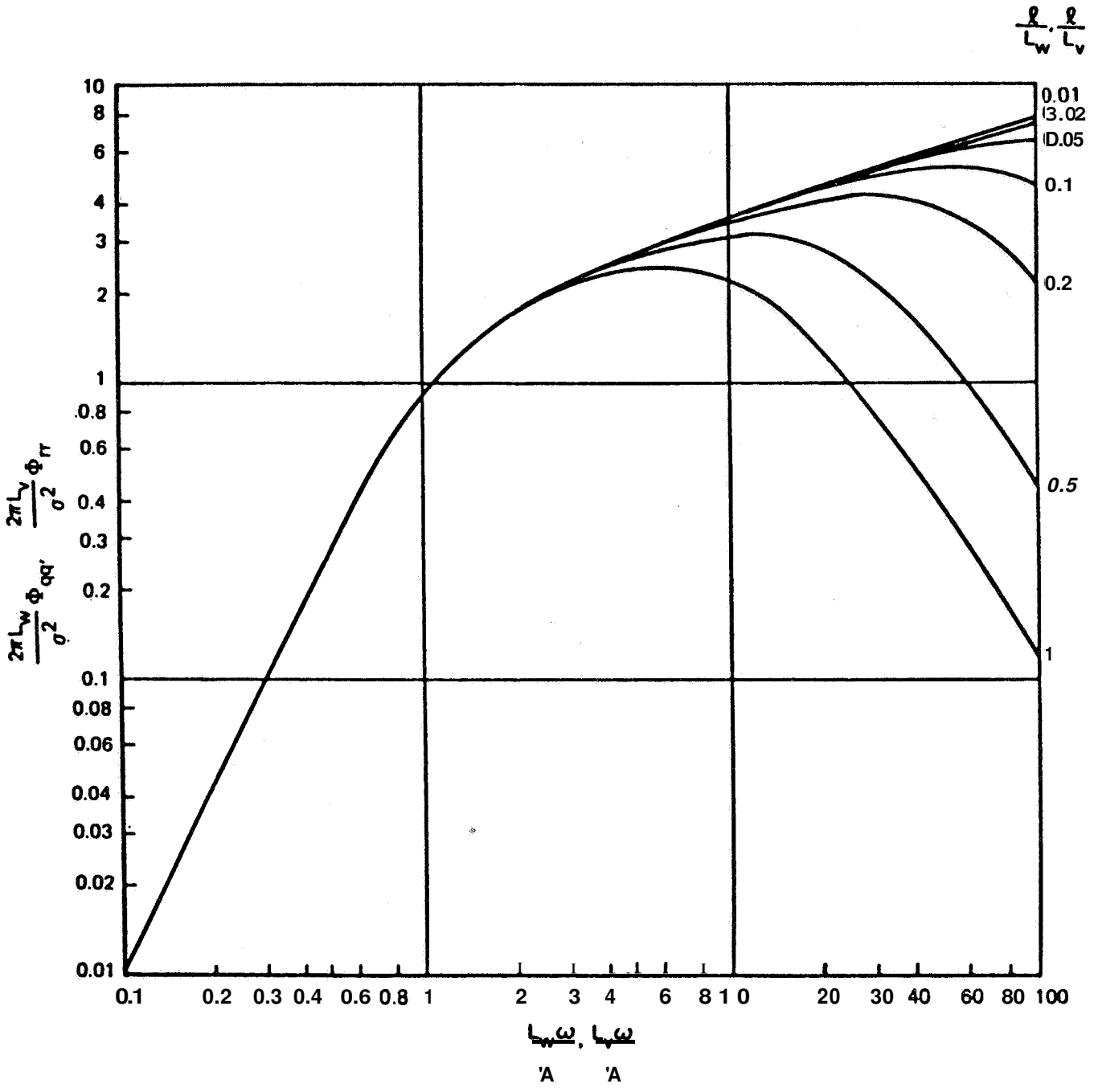

FIGURE 27 – TURBULENCE PITCH AND YAW RATE SPECTRA

$$\dot{u}_T = \frac{\partial u_T}{\partial x}\frac{dx}{dt} = \left[\frac{s}{1 + \frac{4\ell_T}{\pi V_A}s}\right] u_T$$

$$\dot{v}_T = \frac{\partial v_T}{\partial x}\frac{dx}{dt} = \left[\frac{s}{1 + \frac{4\ell_T}{\pi V_A}s}\right] v_T$$

$$\dot{w}_T = \frac{\partial w_T}{\partial x}\frac{dx}{dt} = \left[\frac{s}{1 + \frac{4\ell_T}{\pi V_A}}\right] w_T$$

To accommodate the linear accelerations due to turbulence, the equations for $\dot{\alpha}$ and $\dot{\beta}$ are revised to

$$\dot{\alpha} = \frac{u_A \dot{w}_A - w_A \dot{u}_A}{u_A^2 + w_A^2}$$

$$\dot{\beta} = \frac{(u_A^2 + v_A^2)\dot{v}_A - v_A(\dot{u}_A u_A + w_A \dot{w}_A)}{V_A^2 \sqrt{u_A^2 + v_A^2}}$$

where:

$$\dot{u}_A = \dot{u} - (\bar{\dot{u}}_W + \dot{u}_T)$$

$$\dot{v}_A = \dot{v} - (\bar{\dot{v}}_W + \dot{v}_T)$$

$$\dot{w}_A = \dot{w} - (\bar{\dot{w}}_W + \dot{w}_T)$$

For the representation of the longitudinal distribution of turbulence only (gust penetration), there is an alternate technique based on the frozen field hypothesis. The turbulence velocities may be considered to be frozen

with respect to the air mass as rates of change of turbulence velocities are small compared to the speed and dimensions of an aircraft. The turbulence velocities that strike the airplane at its center of gravity will occur at the tail a time $\Delta t = \ell_T/V_A$ later. The turbulence at the tail may be represented on a digital simulator by storing turbulence velocities occurring at the cg for the appropriate time lag, then using them for turbulence velocities at the tail. If digital noise generation is used, two identical random number sequences displaced in time by $\Delta t = \ell_T/V_A$ may be used. Alternately, linear filter representations for a transport lag may be used. Separate buildups of angle of attack, sideslip angle, and dynamic pressure are provided for the tail, and the forces and moments due to the tail are built up separately from those due to the wing-body.

The highest frequency to which gust penetration is accurate using the transport lag method is

$$\omega < 0.1 \frac{V_A}{\bar{c}}$$

which may not be as good as the restriction for the linear distribution method of

$$\omega < 0.5 \frac{V_A}{\ell_T}$$

The two methods may be combined by separate wing and tail representations using the transport lag plus a linear distribution representation for the wing. The maximum frequency then increases to

$$\omega < \frac{V_A}{\ell_T}$$

The need to provide more and more accurate representations, or rather the sufficiency of any approximation, depends on whether the variance of airplane motion parameters are significantly altered. Approximations that can be shown to be conservative may be acceptable for certification but provide economic penalties due to overdesign. Care must be taken to demonstrate the suitability of assumptions. As the airplane descends, the frequency at which the greatest turbulent energy occurs changes by a factor of 50, drastically altering the response of the airplane. Generally, the lower the speed of an airplane, the more accurate the representation required and the greater the coupling between forces and moments along one coordinate with wind and turbulence components along another coordinate.

WIND MODEL FOR AUTOMATIC LANDING SYSTEM CERTIFICATION

The applicant should account for the aerodynamics of the airplane being evaluated including aeroelasticity, plus the distributed lift effects of steady winds and the longitudinal distribution of lift due to turbulence, unless it can be shown that these effects are insignificant.

The surface mean wind is defined as that at 20 feet above the ground. The automatic landing system need not be certified for surface wind speeds exceeding 25 knots nor for tailwind components exceeding 10 knots. The probability distribution of surface wind speeds ($\overline{V}_{20}$) is presented in Figure 7. The probability distribution for the direction to which the wind is blowing, ($\overline{\psi}_W$), is presented in Figure 17 and is uncorrelated with the surface wind speed. The probability distribution of atmospheric stability as defined in terms of Richardson's number, ($R_{i_{20}}$), is correlated with wind speed and is presented in Figures 13 and 14. The

stochastic combinations of surface wind speed and heading and atmospheric stability may be generated by the model in Figure 28.

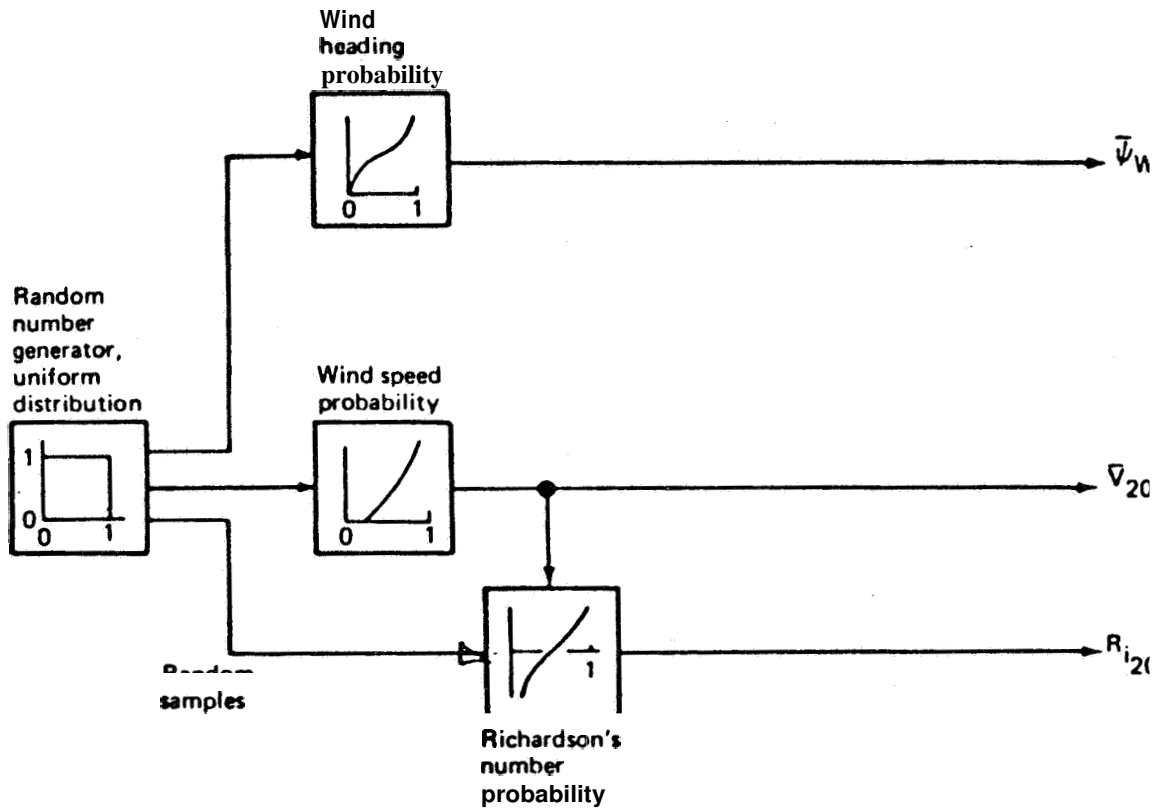

FIGURE 28 – PROBABILITY MODEL SCHEMATIC

The mean wind at any altitude is computed from the equation:

$$\bar{V}_W(h) = \bar{V}_{20}\left(\frac{u_{*_0}/k}{\bar{V}_{20}}\right)\left[\ln\left(\frac{h}{0.15}\right) + f(h/\ell') - \frac{h}{d}g(h/\ell')\right]$$

where

$\frac{u_{*_0}/k}{\bar{V}_{20}}$ is given on Figure 1-7 as a function of $R_{i_{20}}$

$$d = 800 \frac{u_{*_0}/k}{\bar{V}_{20}} \bar{V}_{20}$$

$h \leq d$ no matter what the actual altitude

$1/\ell'$ is given in Figure 29 as a function of $R_{i_{20}}$

$f(h/\ell')$, $g(h/\ell')$ are described in Figures 3 and 8, respectively.

The mean wind shear at any altitude, needed only to define the distributed lift effects of the mean wind, is given by

$$\frac{\bar{V}_W}{h}(h) = \frac{\bar{V}_{20}}{h} \left(\frac{u_{*_0}/k}{\bar{V}_{20}} \right) \left(1 - \frac{h}{d} \right) \phi \left(\frac{h}{\ell'} \right)$$

where $\phi(h/\ell')$ is described in Figure 2 and where, once again, $h \leq d$ no matter what the actual altitude.

The power spectra for uncorrelated components of turbulence in an axis system parallel to the earth but aligned to the direction of the airplane's airspeed vector are given by

$$\Phi_u(\omega) = \frac{\sigma_H^2 L_H}{\pi V_A} \frac{1}{\left[1 + (1.339\ L_H\omega/V_A)^2\right]^{5/6}} \sim \frac{(ft/sec)2}{rad/sec}$$

$$\Phi_v(\omega) = \frac{\sigma_H^2 L_H}{2\pi V_A} \frac{1 + 8/3(1.330\ L_H\omega/V_A)^2}{\left[1 + (1.339\ L_H\omega/V_A)^2\right]} \sim \frac{(ft/sec)}{rad/sec}$$

$$\Phi_w(\omega) = \frac{\sigma_V^2 L_V}{2\pi V_A} \frac{1 + 8/3(1.339\ L_V\omega/V_A)^2}{\left[13(1.339\ L_V\omega/V_A)^2\right]^{11/6}} \sim \frac{(ft/sec)^2}{rad/sec}$$

where the spectra are defined such that

$$\sigma_H^2 = \int_{-\infty}^{\infty} \Phi_u(\omega)\, d\omega = \int_{-\infty}^{\infty} \Phi_v(\omega)\, d\omega$$

= variance of a horizontal component of turbulence

$$\sigma_w^2 = \int_{-\infty}^{\infty} \Phi_u(\omega)\, d\omega$$

= variance of the vertical component of turbulence

and where

$$\sigma_V = 0.4\bar{V}_{20} \left(\frac{u_{*0}/k}{\bar{V}_{20}} \right) \left(1 - \frac{h}{d} \right) \left(\frac{\sigma_V}{u_*} \right)$$

$\frac{\sigma_V}{u_*}$ defined on Figure 23 is a function of h/ℓ'

$$\sigma_H = \left(\frac{\sigma_H}{\sigma_V} \right) \sigma_V$$

$\frac{\sigma_H}{\sigma_V}$ given as function of altitude on Figure 25.

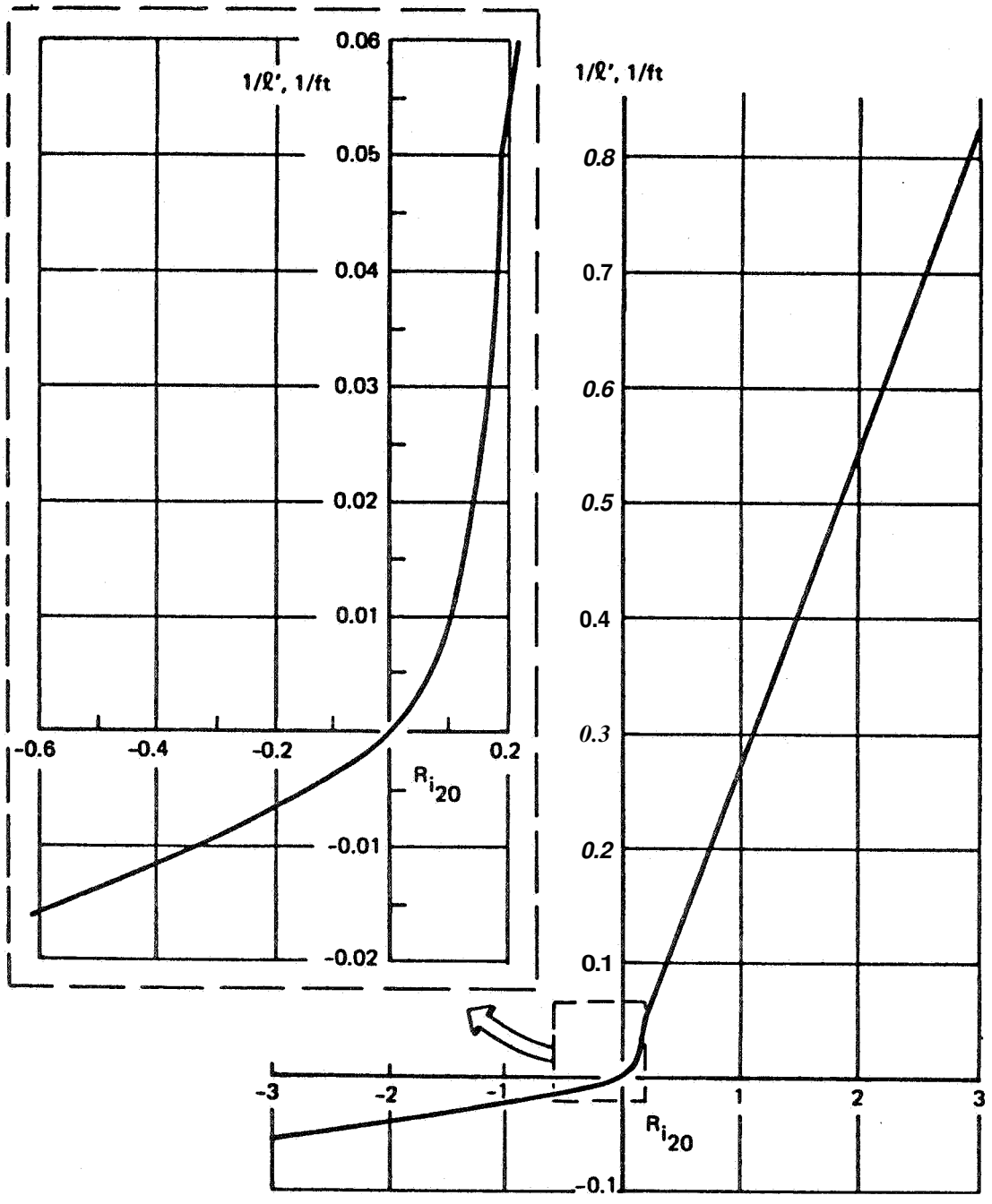

FIGURE 29 – SCALING LENGTH

$$L_V = \begin{cases} h & , h < 1000 \text{ ft} \\ 1000 \text{ ft} & , h \geq 1000 \text{ ft} \end{cases}$$

$$L_H = L_V(\sigma_H/\sigma_V)^3$$

The spectra are well represented by generating turbulence components equal to passing uncorrelated Gaussian white noise through the filters in Figure 20.

Body axis components of mean wind, mean wind shear, and turbulence are found by means of the transformations in Figure 16.

The interrelationships between the components of the wind model and the other elements of the simulation are described in Figure 30.

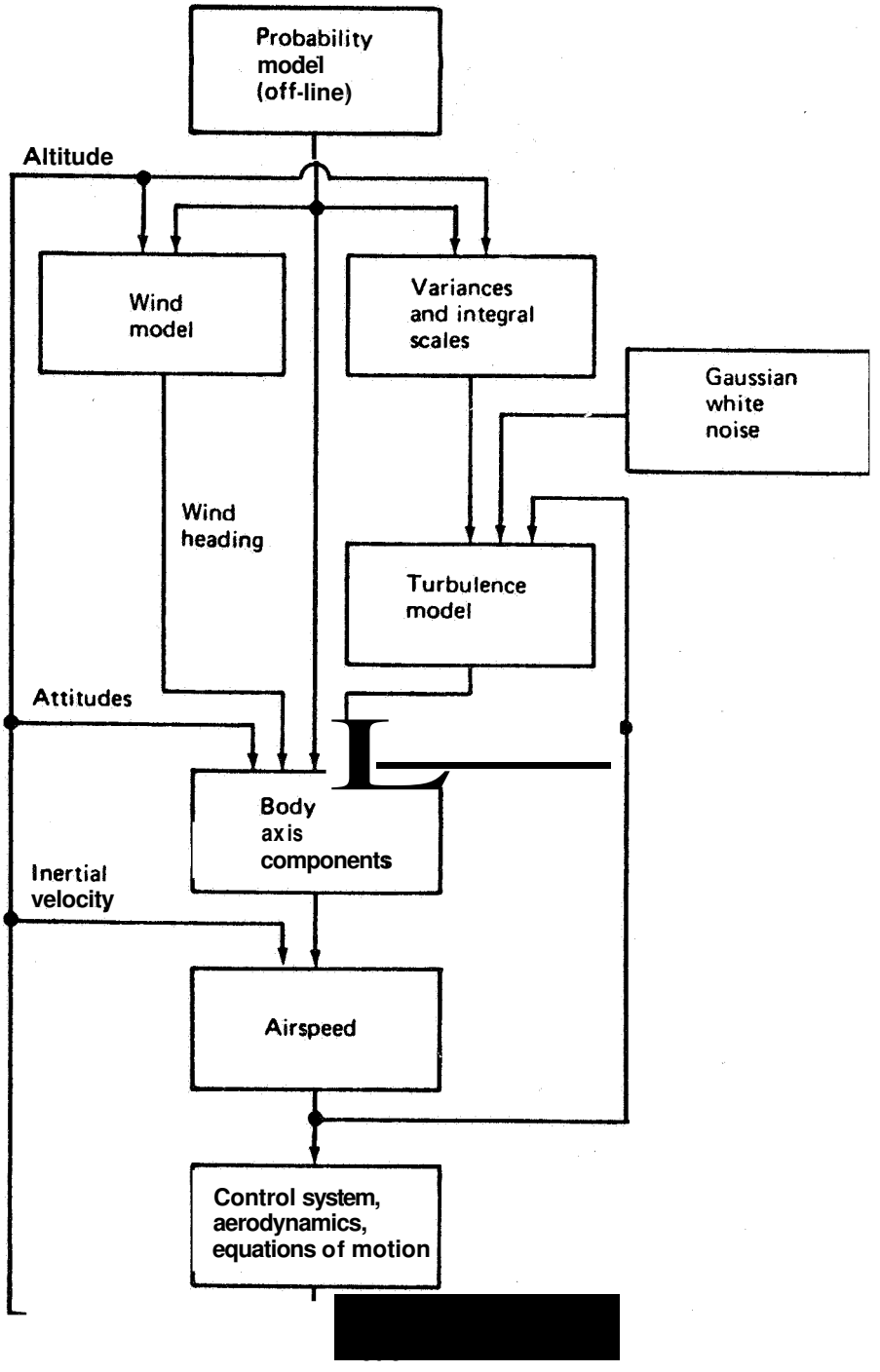

FIGURE 30 –COMPUTATION FLOW DIAGRAM